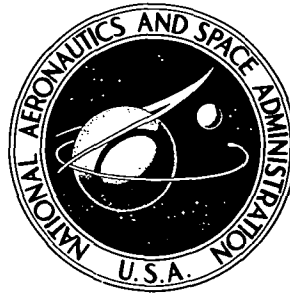


NASA TECHNICAL NOTE



N73-29480
NASA TN D-7307

NASA TN D-7307

CASE FILE
COPY

COLD CATHODES FOR SEALED-OFF CO₂ LASERS

*by Urs E. Hochuli, Thomas P. Sciacca,
and Charles R. Hurt*

*Goddard Space Flight Center
Greenbelt, Md. 20771*

1. Report No. NASA TN D-7307	2. Government Accession No.	3. Recipient's Catalog No.	
4. Title and Subtitle Cold Cathodes For Sealed-Off CO ₂ Lasers		5. Report Date August 1973	
		6. Performing Organization Code 733	
7. Author(s) U. Hochuli, T. Sciacca, and C. Hurt		8. Performing Organization Report No. G-7332	
9. Performing Organization Name and Address Goddard Space Flight Center Greenbelt, Maryland 20771		10. Work Unit No. 604-42-01-01	
		11. Contract or Grant No.	
		13. Type of Report and Period Covered Technical Note	
12. Sponsoring Agency Name and Address National Aeronautics and Space Administration Washington, D. C. 20546		14. Sponsoring Agency Code	
15. Supplementary Notes			
16. Abstract <p>Experimental results of a group of theoretically selected cold cathode materials are presented. These tests indicate Ag-CuO, Cu, and Pt-Cu as three new cold cathode materials for sealed-off CO₂ lasers. The power output of a test laser with an Ag-CuO cathode and a gas volume of only 50 cm³ varied from 0.72 W to 1.1 W at 3000 hours and still yields 0.88 W after 8000 hours. Gas discharge tubes with Cu cathodes and a volume of 25 cm³ yield lifetimes in excess of 10,000 hours. Gas analysis results, obtained from a similar tube over a period of 3000 hours, look most promising. A Pt-Cu alloy cathode shows an extremely promising V-I characteristic over a period of 2800 hours.</p>			
17. Key Words (Selected by Author(s)) Communications, CO ₂ Laser, Cold Cathodes, 10 ⁴ Hour Life, 1-W Sealed-off CO ₂ Laser; Gas Mixture Optimization		18. Distribution Statement Unclassified - Unlimited	
19. Security Classif. (of this report) Unclassified	20. Security Classif. (of this page) Unclassified	21. No. of Pages 60	22. Price* \$3.00

* For sale by the National Technical Information Service, Springfield, Virginia 22151

CONTENTS

	Page
ABSTRACT	i
INTRODUCTION	1
CATHODE PARAMETERS INVOLVED	1
EXPERIMENTAL APPROACH	3
Gas Analysis	3
Experimental Techniques	4
EXPERIMENTAL RESULTS	4
Gold Cathodes	4
Silver Cathodes	4
Silver Matrix Cathodes	5
Ag-CdO Cathodes	5
Ag-CuO Cathodes	5
Ag-MnO ₂ Cathodes	5
Ag-NiO Cathodes	5
Ag-ZnO Cathodes	6
Copper Cathodes	6
Oxide Layer Cathodes	6
Platinum Cathodes	6
Palladium Cathodes	7
Nickel Cathodes	7
CATHODE ALLOYS TESTED	7
LASERS	9
CONCLUSION	10
ACKNOWLEDGMENTS	10

(Contents continued)

	Page
REFERENCES	11
APPENDIX—LASER V-I CHARACTERISTICS FOR DIFFERENT GAS MIXTURES	47

COLD CATHODES FOR SEALED-OFF CO₂ LASERS

Urs E. Hochuli

University of Maryland

Thomas P. Sciacca and Charles R. Hurt

Goddard Space Flight Center

INTRODUCTION

Most of the gas discharge tubes used for CO₂ lasers are high-impedance devices requiring only small currents; cold cathodes are suitable electron emitting sources to furnish these currents. Gas removal due to cathode sputtering usually limits the life of discharge tubes filled with noble gases. Moreover, dissociation of CO₂ into CO and O₂ with successive oxygen removal due to oxide layer formation is a consideration for the CO₂ laser. The degree of dissociation is very much influenced by the cathode surface chosen. It is a difficult problem to find the proper cathode materials that do not remove gas by sputtering and avoid consumption of any gas mixture constituent through scale formation.

The CO₂ laser was discovered in 1964.¹ Its high efficiency and power capability make it ideal for communication purposes as well as for energy sources. Despite the recognition of its importance we have so far had no entirely satisfactory cold cathode for the CO₂ laser. It is true that the state-of-the-art has been much advanced in the last two years, but we are still looking for a cathode that is noise free, does not produce sputtering deposits, and lasts for 10,000 hours or more with small gas volumes. The nickel cathode invented by Dr. Carbone,² the platinum cathode discovered by Dr. Whitemann,³ and the NiO cathode developed by Honeywell depend on a relatively large gas volume and can yield lifetimes of several thousand hours under this condition. Used in a 1-W CO₂ laser with a typical gas volume of the order of 50 to 100 cm³ they usually last less than 1000 hours. The demand for a space-qualified laser tube with a life expectancy of at least 2000 hours has justified the need for CO₂ laser cold-cathode research. These facts also indicate that we are dealing with a difficult and important unsolved problem.

CATHODE PARAMETERS INVOLVED

Sealed-off CO₂ lasers are relatively tolerant of the composition of the gas mixture used. One of the most efficient mixtures uses He-CO₂-N₂-Xe. It has been shown by several researchers⁴ that CO can be substituted for N₂. We have optimized one of our own 1-W lasers with respect to gas composition, and the results are shown by Figures 1 to 22. From these measurements we must conclude that the substitution of CO for N₂ has little effect on power output. For example, we measure a power output of 1.3 W at 6 mA and 5100 V across the laser tube for a gas mixture containing 9.1 Torr He, 4.25 Torr CO₂, 5.45 Torr

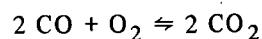
CO, and 1.2 Torr Xe. This result must be compared with a power output of 1.2 W obtained at 6 mA and 4980 V across the laser tube for a mixture consisting of 10 Torr He, 4.65 Torr CO₂, 4.65 Torr N₂, and 0.7 Torr Xe. For these two cases the substitution of CO for N₂ gave a slightly larger power output and also a slightly higher efficiency. We have to mention that our results have been measured during the first ten minutes the laser was turned on and do not reflect long-term changes in the composition of the gas mixture. The laser tube for our measurements originally gave an output of 1.7 W, and successive cathode tests produced a slight, visible layer of deposits on the internal gold-coated mirror. These deposits reduced the power output from 1.7 to 1.3 W under otherwise identical conditions.

It has also been shown that a small amount of H₂ or H₂O can be added, and this may further increase power output and efficiency.⁵ Our own incomplete measurements for H₂ addition are shown in Figures 23 to 26. These variations in the gas composition are not only important for the achievement of maximum power output or efficiency, they also profoundly affect the cathode chemistry and therefore the life of the laser tube. The other parameters of the cathode are the current density, the temperature, and the composition of the cathode surface. The current density can, to a certain extent, be controlled by the choice of the cathode geometry. We have normalized the cathodes, which were designed for a current of 6 mA, to four diameters to conform to available or easily modified ceramic sputter shields. These normalized cathode configurations are shown in Figure 27.

The operating temperature of these cathodes depends, of course, on the current, and the temperature can be raised by using thermal insulation outside of the cathode sleeve. Typical temperatures for one cathode configuration are shown in Figure 28. The last parameter, the composition of the cathode surface, is dealt within the next paragraph.

We would like to find cathode materials that are chemically inert in the presence of the particular gas mixture used. We also require a very low sputtering rate of the materials used for the cold-cathode surface, and the last requirement asks for a minimum of negative ion formation in the sputtering products. This is necessary to prevent material deposits at the anode end due to the attraction of such negative ions by the positive anode.

Of particular interest are the metal-oxides with a larger oxygen dissociation pressure than the one of the reaction



Some of these oxides are shown in the standard free-energy diagram in Figure 29 located above the reaction mentioned. The dissociation O₂ pressure can be read from this diagram or from Figure 30. In the presence of a mixture of equal parts CO and CO₂ these oxides are reduced to their lower oxidation state under condition of thermal equilibrium and in the absence of the electrical discharge current. (It is noteworthy that most of these metals and oxides also act as catalysts for the CO oxidation reaction. The fact that the degree of CO₂ dissociation is indeed affected by the cathode surface chosen is

also documented in the literature.⁶) The use of one of these materials as a cold cathode exposes it to additional processes such as ion bombardment, photo-, field-, and thermal-emission, with the result that the surface has a tendency to stay in the higher oxidation state. Oxidation at the cathode end of discharge tube is unexpected but has been observed and described.⁷

The discharge conditions of most of the small CO₂ lasers result in cathode current densities above 2 mA/cm². Experience shows that insulating oxide layers can usually not support such current densities over prolonged periods of time. This difficulty can be avoided by using semiconducting oxide layers. Most of the oxides under consideration are of this type and their electrical conductivity as well as their catalytic activity increase with temperature. Unfortunately, reliable data of electrical conductivity of oxides versus temperature is rather scarce in the recent literature.

EXPERIMENTAL APPROACH

It was obvious from the beginning of the research that a large number of different cathode materials had to be tested. To build a laser for each different cathode would have been prohibitively expensive in terms of manpower, materials expenses, and testing facilities. A faster and far cheaper approach was to test gas discharge tubes alone. This was done and the standard geometry chosen for the discharge tubes is shown in Figure 31. Discharge voltage measured at constant current and color of the discharge versus time are coarse and not always sufficient indicators of the condition of the tubes. We felt that at least a partial gas analysis was necessary to verify the composition of the gas mixture over the life-span of the most promising discharge tubes. This can be achieved either by periodically analyzing gas samples in the mass-spectrometer or by infrared absorption spectroscopy. We have chosen infrared absorption spectroscopy to obtain an indication of the CO₂ and CO content of the tubes. This required the attachment of an absorption cell with infrared transmitting windows to each discharge tube. The cell geometry chosen increased the gas volume of the discharge tube from roughly 25 cm³ to 50 cm³. The most successful cathodes were then tested in actual lasers.

Gas Analysis

As previously mentioned, the CO and CO₂ content was monitored with infrared absorption spectroscopy. The absorption cells had a path length of 7.8 cm and 1-mm thick Irtran-2 windows; their geometry is shown in Figure 32. The absorption spectrum between 2000 and 2500 cm⁻¹ was measured with a DigiLab model FTS 14 double-beam spectrometer. The resolution of this instrument is insufficient to display the true line shape of a single rotational CO₂ or CO line. For this reason we chose an equivalent slit width that would enable us to sample over two or more rotational lines. A slit width of 8 cm⁻¹ achieves this objectively, saves time, and was chosen for all measurements. Figure 33 shows a sample spectrum of the reference mixture of 20 Torr He CO₂ CO X_e in the pressure ratios

15:7:7:1 and indicates maximum absorption of roughly 10 percent for CO₂ and 1.2 percent for CO. Further measurements were made with expanded scales, Figure 34, and the results for other gas compositions are shown in Figures 35 to 40.

Experimental Techniques

All the discharge tubes and lasers were made from Pyrex and had tungsten electrode feed-throughs. Gallium arsenide and Irtran-2 windows as well as the internal gold-coated quartz mirrors were attached with indium film seals developed for this purpose in our laboratory.⁸ All these seals are of the ultrahigh vacuum type and no Epoxy resin was used anywhere. The tubes were evacuated with an oil diffusion pump and the electrodes outgassed with RF generator and torch. The first discharge was usually in pure oxygen followed by a burn-in period of one to two days in the final mixture. Subsequently, the tubes were refilled, sealed off, and run on the test stand. Practically all the cathode alloys were fabricated in our own laboratory and then cast and machined or rolled and formed into the final shape. Internal oxidation of the silver alloys was performed in a temperature-controlled furnace with a quartz tube flushed with O₂ as a working chamber.

EXPERIMENTAL RESULTS

From the oxygen dissociation curves in Figure 30 we see that gold forms the most unstable oxides, followed by silver, MnO₂, PtO, PdO, and CuO.

Gold Cathodes

We would expect that gold, the most noble metal with respect to oxidation, would be a rather inert cathode surface. Unfortunately, gold sputters very badly and we have so far not been able to get reasonable life with such cathodes in He-CO₂-N₂-Xe mixtures.

Silver Cathodes

The next noble metal, silver, does not work successfully in the He-CO₂-N₂-he mixtures probably because the volatile Ag NO₃ can be formed. In He-CO₂-CO-Xe mixtures we see an entirely different picture. Here we can observe how the discharge oxidizes the spot of impact at the cathode. This area becomes dark due to silver oxide formation, with a resulting local decrease in the electrical conductivity. This lowered electrical conductivity then forces the cathode spot to move to an unoxidized area. If the cathode has a temperature of 200° to 300° C we can later observe how the original, oxidized area returns again to pure silver by dissociation. Such cathodes can have quite a long life and some of them are surprisingly sputter-free. Their drawback is the electrical instability caused by the moving cathode spot. Typical characteristics are shown in Figure 41.

We have also tried to reduce the surface resistivity of the oxide layer by increasing the temperature. This attempt was unsuccessful and usually resulted in increased sputtering.

Another method is to alloy the silver with a metal that forms oxides with a higher electrical conductivity. The additional metal in the alloy has to be oxidized in order to prevent oxygen depletion in the final gas mixture. This process then leads to:

Silver Matrix Cathodes

Silver at high temperatures is quite transparent to oxygen and for this reason silver alloys can be internally oxidized. The best known examples are probably the Ag-CdO alloys used for electrical contacts. This compound can be formed by sintering compressed Ag-CdO powder slugs or by exposing the Ag-Cd alloy to an oxidizing atmosphere at high temperatures for extended periods of time. We have formed Ag-CdO, Ag-CuO, Ag-MnO₂, and Ag-ZnO cathodes and used sintered Ag-CdO and Ag-NiO cathodes. These cathodes consist essentially of a silver matrix holding the oxide particles. Curves from reference⁹ for the Ag-CuO internal oxidation process are shown in Figure 42. Silver matrix cathodes should be relatively inert to surface damage and free of electrical instabilities once sufficiently low surface resistivity has been achieved.

Ag-CdO Cathodes

Results for these cathodes are shown in Figures 43 to 46. The main sputtering deposits stay close to the cathode; slight anode deposits do occur.

Ag-CuO Cathodes

These cathodes work quite well, as illustrated in Figures 47 to 49, but still show moving cathode spots. Anodes stay very clean and surprisingly low cathode deposits occur with the 2L 4.5 type cathodes. Notice the CO decrease and the CO₂ increase with time for cathodes with 10 percent or more Cu. In these cathodes sputtered CuO is reduced to Cu₂O, giving off oxygen. The partial pressures of CO and CO₂ stayed fairly well balanced for the cathode with 5 percent Cu, while pure Ag cathodes show an excess of CO in Figure 41. Ag-CuO cathodes are not successful in the presence of N₂.

Ag-MnO₂ Cathodes

The cathodes were first oxidized at 750° C and then at 500° C to achieve conversion to MnO₂, known to be an excellent catalyst.¹⁰ Results are shown in Figure 50. Anode deposits do occur with these discharge tubes but the cathode spots are relatively quiet. The cathodes are unsuccessful in the presence of N₂.

Ag-NiO Cathodes

Results are shown in Figure 51. The anodes stay relatively clean and the cathodes are quiet in these discharge tubes.

Ag-ZnO Cathodes

Results are shown in Figure 52. Quiet cathode sport, very light anode deposits. The cathode with 10 percent Zn shows some cathode deposits. These cathodes are unsuccessful in the presence of N_2 .

Copper Cathodes

Oxide layers can be formed in an oxygen discharge and such cathodes live surprisingly long with quite large current densities. It is a known fact that thin oxide layers on Cu grow very slowly at room temperature.¹¹ Anodes stay very clean; cathodes are unsuccessful in the presence of N_2 . Cathode spots move when large current densities are used, but practically no sputtering occurs. Cathode spots are quiet with lower current densities but the sputtering rate is higher. Results are shown in Figure 53.

Oxide Layer Cathodes

Such cathodes can be formed by oxidizing alloys in an oxygen atmosphere for a prolonged period of time at elevated temperatures. The scaling layers so formed usually contain the oxide of the less noble component of the alloy. Suitable layers have to adhere very well, for example, CuO on Au,¹² and are only allowed to continue growing at an infinitesimal rate at the operating temperature of the cathode. Such cathodes are of course much more delicate than matrix cathodes formed by internal oxidation. For this reason we have not stressed their development and only a few were tried.

Platinum Cathodes

Pure platinum cathodes dissociate very little CO_2 ⁶ but sputter badly and are not successful. We have tried to reduce the sputtering by alloying Pt with Ag, Au, Cu, and Ni. The results show that sputtering can indeed be reduced drastically but the life of the discharge tubes tested was generally less than 1000 hours. The addition of hydrogen or water vapor does, however, change the situation. It is well known that platinum oxides can be reduced by atomic hydrogen at room temperature in a cycle similar to the water vapor cycle in incandescent lamps¹³. Langmuir described this cycle as follows:

A lamp made up with a side tube containing a little water which is kept cooled by a freezing mixture of solid carbon dioxide and acetone ($-78.5^\circ C$) will blacken very rapidly when running at normal efficiency, although the vapor pressure of water at this temperature is only about 4×10^{-4} mm.

The explanation [Langmuir states] of the behavior of water vapor seems to be as follows:

The water vapor coming into contact with the filament is decomposed, the oxygen combining with the tungsten and the hydrogen being evolved. The oxide distills to

the bulb, where it is subsequently reduced to metallic tungsten by atomic hydrogen given off by the filament, water vapor being simultaneously produced. The action can thus repeat itself indefinitely with a limited quantity of water vapor.

Several experiments indicated that the amount of tungsten that was carried from the filament to the bulb was often many times greater than the chemical equivalent of the hydrogen produced, so the deposit on the bulb could not well be formed by the simple attack of the filament by water vapor.

Another experiment demonstrated that even the yellow oxide, WO_3 , could be reduced at room temperature by atomic hydrogen. A filament was heated in a well-exhausted bulb containing a low pressure of oxygen; this gave an invisible deposit of the yellow oxide on the bulb. The remaining oxygen was pumped out and dry hydrogen was admitted. The filament was lighted to a temperature (2000 K) so low that it could not possibly produce blackening under ordinary conditions. In a short time the bulb became distinctly dark, thus indicating a reduction of the oxide by the active hydrogen. Further treatment in hydrogen failed to produce any further darkening, showing that the oxide could only be reduced superficially.

Platinum alloy cathodes working with gas mixtures containing hydrogen or water vapor are essentially mass transport cathodes with transport rates controlled by the impurity used. In this case we need far larger impurity concentrations to reduce sputtering, and preliminary results are seen in Figures 54 and 55.

Palladium Cathodes

Just as with Pt, these cathodes seem to be good catalysts but sputter far too much. We have not yet had time to check their behavior with gas mixtures containing H_2 or H_2O .

Nickel Cathodes

The life of discharge tubes using nickel with oxidized or unoxidized surfaces has always been restricted to less than 1000 hours by our test conditions. The substitution of CO for N_2 in the gas mixture did not improve this result.

CATHODE ALLOYS TESTED

These are shown in Tables 1 and 2.

Table 1
 Impurity Percent by Weight of Cathode Alloys Tested in He-CO₂-N₂-Xe.
 15/7/7/1 Gas Mixtures.

Main Element Impurity	Ag	Au	Co	Cu	Mn	Ni	Pd	Pt	Re
Ag	100			3			1,3,10	1,3	
Au		100					10	3,10	
Cd	0.8,2 5,10,20								
Co									
Cu	20			100	38		3,7 10,14	0.3,1, 3,10, 30	
Mn	0.5,3 5,10		0.5,2 10						
Ni	15						3	0.2, 0.5,1, 1.5,2, 2.5,3, 6,10	
Pd							100		
Pt	3,10					10		100	
Re									100
Zn	10								

Table 2
 Impurity Percent by Weight of Cathode Alloys Tested in He-CO₂-CO-Xe.
 15/7/7/1 Gas Mixtures.

Main Element Impurity	Ag	Au	Co	Cu	Mn	Ni	Pd	Pt	Re
Ag	100	10						1,3	
Au	18	100						1,10	
Cd	1,10								
Co			100						
Cu	5,10,20	5		100	38				
Mn	1.25 3,10			2,10		10			
Ni	15		40			100		0.5 1,2	
Pd	10,18								
Pt	3,26							100	
Re									100
Zn	1,3,10								

LASERS

A typical result for a laser with a nickel cathode is shown in Figure 56. Far more encouraging is the power output versus time of the laser with a 1 L 4.5 Ag 20 Cu/O cathode shown in Figure 57. This cathode is actually somewhat too small and has worked with a larger than optimum current density. As a result of this sputtering has taken place, but the deposits are nicely confined to the cathode area. The most impressive fact is the lack of visible deposits in the bore, on the anode, or on the gold-coated internal mirror at the anode end after 8000 hours of continuous service. The sputtering in the cathode area is almost completely eliminated with the next larger 2 L 4.5 type cathode. Comparison

of the last two results shows that indeed much progress has been made during the past year.

CONCLUSION

From the many test results available we see that careful selection of gas mixture composition, cathode material, and geometry promise CO₂ laser life of 10,000 hours or more. So far Ag-CuO and pure Cu cathodes are the most successful ones in combination with the He-CO₂-CO-Xe mixture. Both of these cathodes show a minimum of sputtering deposits in the bore and on the anode. To date we have not been able to completely suppress the flickering of the cathode spot in the Ag-CuO cathodes. Pure Cu cathodes show the same effect for current densities above 18 mA/cm². Lowering the current density to 12 mA/cm² stabilizes these cathodes at the expense of increased sputtering. The sputtering products are still confined to the cathode area, and if the results of the gas analysis continue to confirm the excellent appearance of the 10,000 hour-old discharge tubes, we may very well have the best overall results with the pure Cu cathode. This solution would also be very attractive from the point of view of simplicity: namely a simple cathode working with the least complicated efficient gas mixture available.

Surprisingly good discharge characteristics are shown in Figure 55 for a Pt cathode alloy containing 30 percent Cu in combination with a He-CO₂-N₂-Xe gas mixture. This result has to be reproduced and confirmed by gas analysis. The cathode itself seems to be electrically quiet but produces anode deposits. Much more experience is needed with this cathode type and we are exploring the influence of the composition of the Pt-Cu alloy. However, from an engineering point of view we have some reservations. The addition of a small amount of H₂ or H₂O very much increases the complexity of the cathode problem. New chemical compounds can be formed and it is of course very well known that the control of the hydrogen pressure depends to a certain extent on the surface properties of the materials used for the fabrication of the laser tube.

ACKNOWLEDGMENTS

This work was initiated at the University of Maryland by fundings from ONR, ARPA, and continued by NASA. Some of the CO and CO₂ absorption measurements are from part of Carvel Holton's master's thesis which is in preparation.

Goddard Space Flight Center
National Aeronautics and Space Administration
Greenbelt, Maryland, February 9, 1973
604-42-01-01-51

REFERENCES

1. C. K. N. Patel, W. L. Faust, and R. A. McFarlane. "CW Laser Action on Rotational Transitions of the $\Sigma_u^+ - \Sigma_g^+$ Vibrational Band of CO_2 ." *Bull. Am. Phys. Soc.*, **9**. April 27, 1964. p. 500.
2. R. J. Carbone. "Long-term Operation of a Sealed CO_2 Laser." *IEEE J. Q. E.*, Vol. QE-3. September 1967. pp. 373-375.
3. W. J. Witteman. "Increasing Continuous Laser Action on CO_2 Rotational Vibrational Transitions through Selective Depopulation of the Lower Laser Level by Means of Water Vapor." *Phys. Letters*, **18**. August 15, 1965. p. 125.
4. Norio Karube and Eiso Hamaka. "Decomposition of CO_2 Molecules in a Sealed CO_2 Laser." *J. Appl. Phys.*, **9**. 1969. p. 3883.
5. W. J. Witteman and H. W. Werner. "The Effect of Water Vapor and Hydrogen on the Gas Composition of a Sealed-Off CO_2 Laser." *Phys. Letters*, **26A**. April 1968. p. 454.
6. E. N. Lotkova, V. N. Ochkin, and N. N. Sobolev. "Dissociation of Carbon Dioxide and Inversion in CO_2 Laser." *IEEE J. Q. E.*, **7**. 1971. p. 396.
7. D. V. Ignatov. "Recherches Électronographiques sur les Pellicules d'Oxydes Apparaissant sur l'Aluminium et le Nickel dans une Décharge Électrique en Milieu Gazeux d'Oxygène." *J. Chim. Phys.*, **54**. 1957. p. 96.
8. U. Hochuli and P. Haldemann. "Indium Sealing Techniques." *Rev. Sci. Instr.*, **43**. 1972. p. 1088.
9. Ernst Raub and Max Engel. "Zundern Kupferhaltiger Legierungen der Edelmetalle." *Z. f. Metallkunde*, **38**. 1938. p. 83.
10. M. Katz. *Advances in Catalysis*. Academic Press, Inc., New York, 1953.
11. Jacques Bénard. *L'Oxidation des Métaux*, Vol. 1. Gauthier-Villars and Co., Paris, 1962. p. 126.
12. O. Kubachewski. "Das Verhalten von Platin-und Goldlegierungen mit Kupfer." *Z. Elektrochem.*, **49**. 1943. p. 451.
13. S. Dushman and J. M. Lafferty. *Scientific Foundations of Vacuum Technique*, 2nd ed., John Wiley and Sons, Inc., New York, 1967. p. 647.

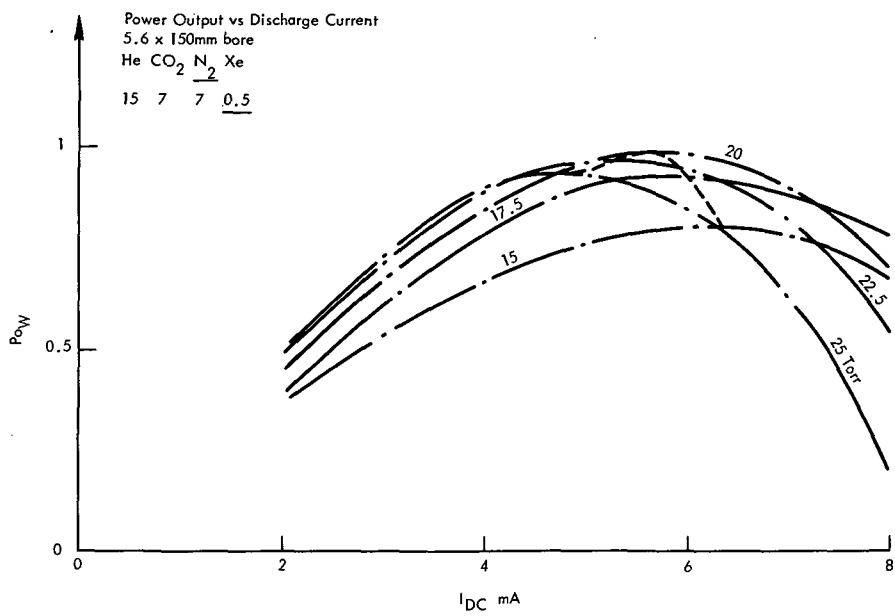


Figure 1. Power output as a function of discharge current [Po(W) versus I_{DC} (mA)] for a 150-mm length laser tube with a 5.6-mm bore.

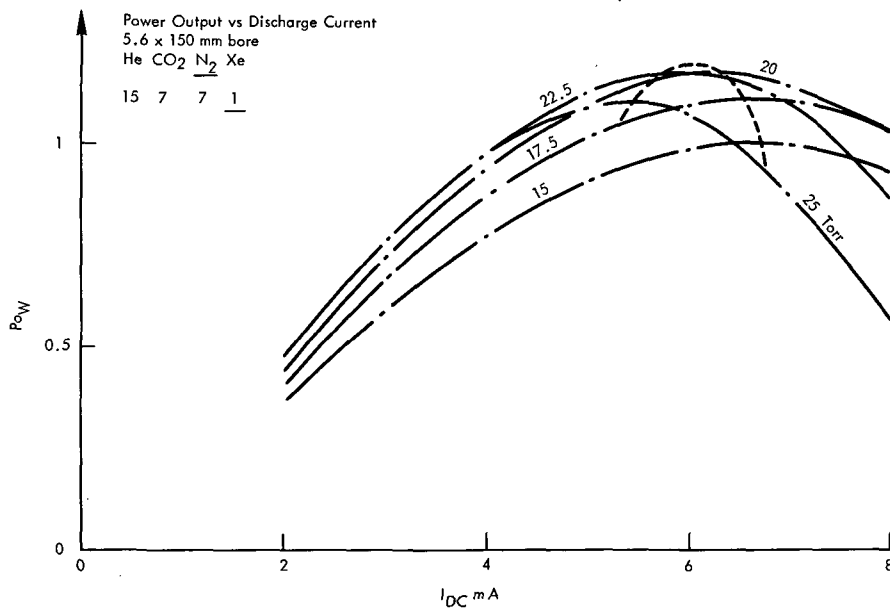


Figure 2. Power output as a function of discharge current [Po(W) versus I_{DC} (mA)] for a 150-mm length laser tube with a 5.6-mm bore.

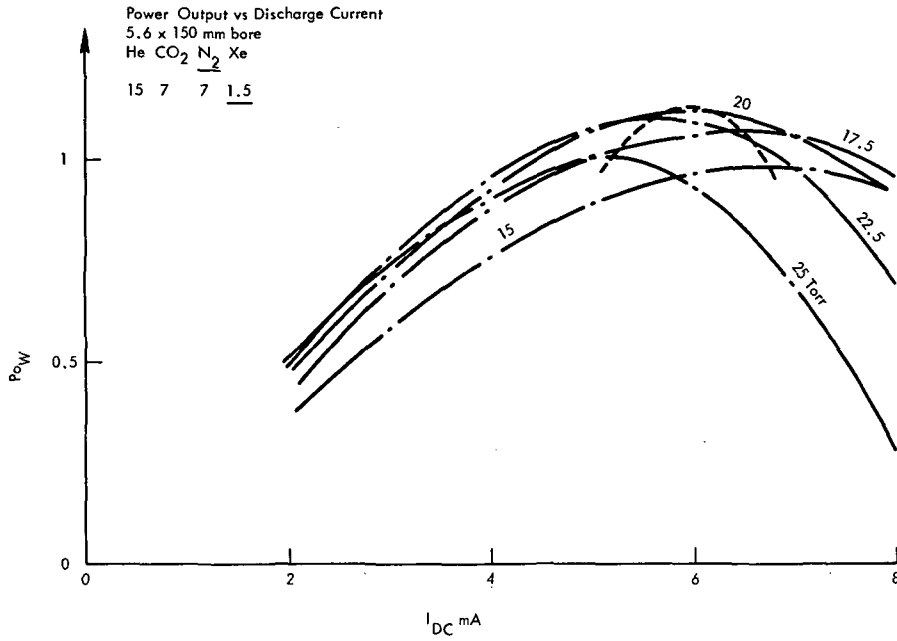


Figure 3. Power output as a function of discharge current [$P_o(W)$ versus I_{DC} (mA)] for a 150-mm length laser tube with a 5.6-mm bore.

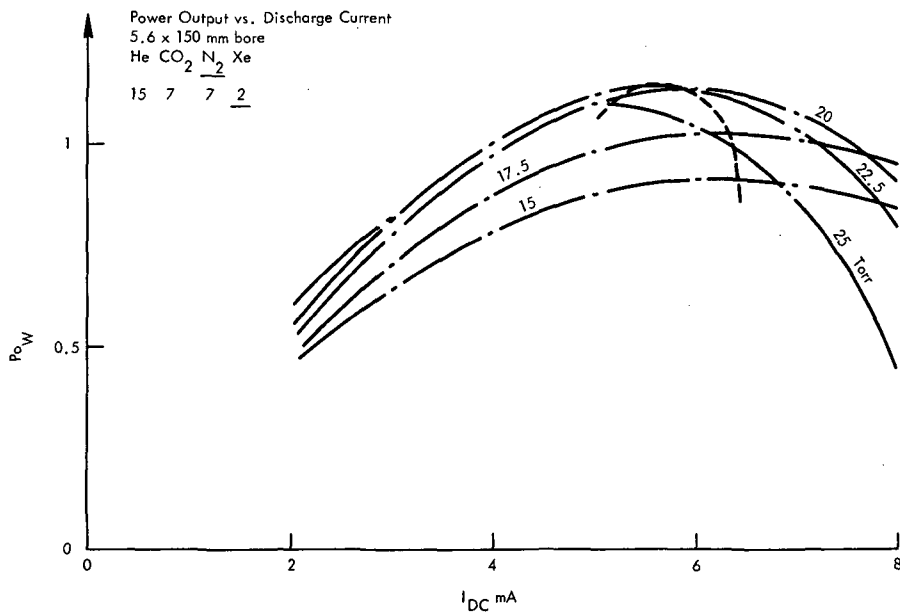


Figure 4. Power output as a function of discharge current [$P_o(W)$ versus I_{DC} (mA)] for a 150-mm length laser tube with a 5.6-mm bore.

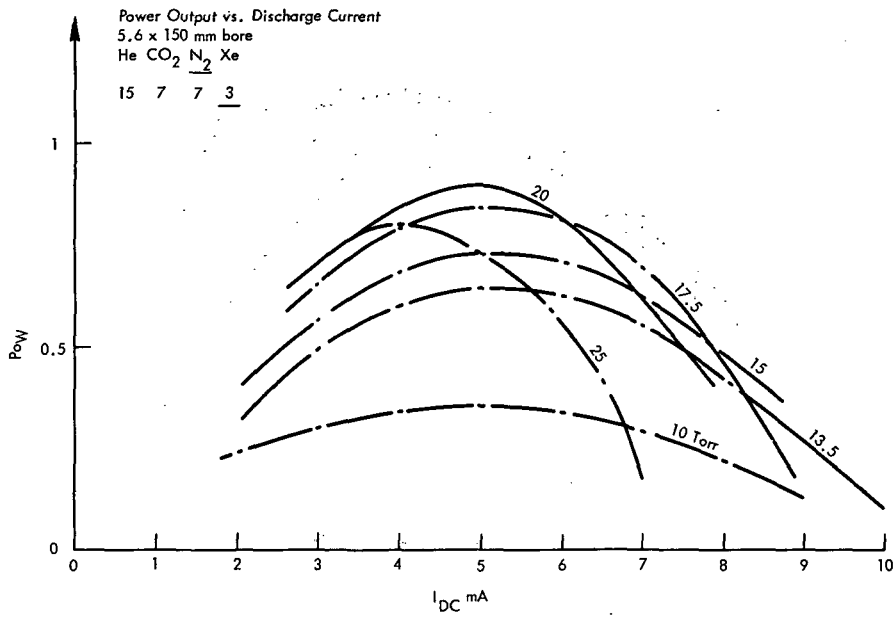


Figure 5. Power output as a function of discharge current [Po(W) versus I_{DC} (mA)] for a 150-mm length laser tube with a 5.6-mm bore.

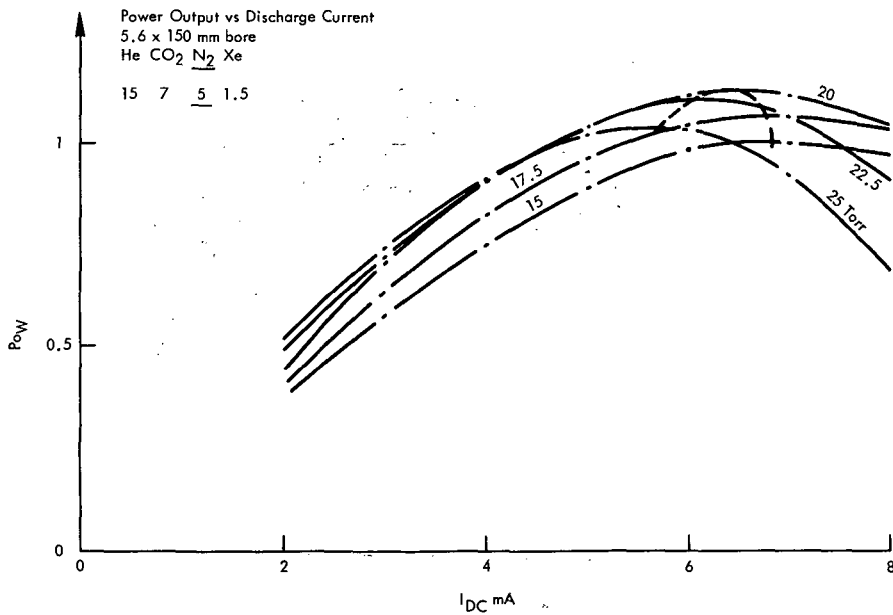


Figure 6. Power output as a function of discharge current [Po(W) versus I_{DC} (mA)] for a 150-mm length laser tube with a 5.6-mm bore.

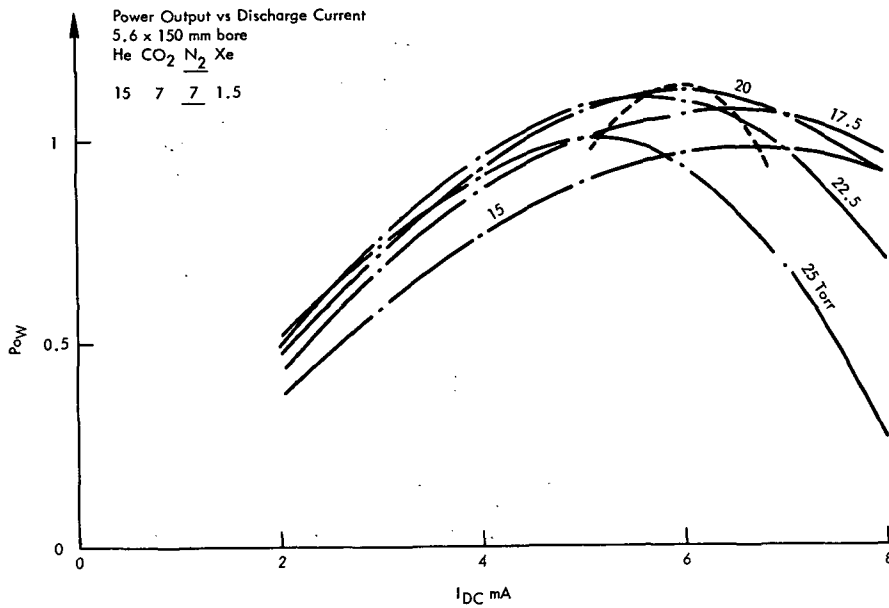


Figure 7. Power output as a function of discharge current [Po(W) versus I_{DC} (mA)] for a 150-mm laser tube with a 5.6-mm bore.

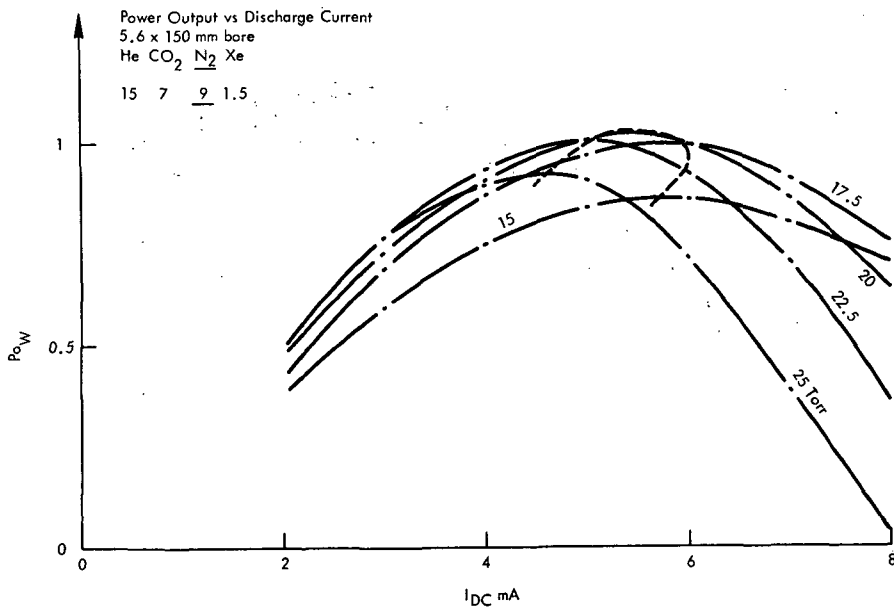


Figure 8. Power output as a function of discharge current [Po(W) versus I_{DC} (mA)] for a 150-mm length laser tube with a 5.6-mm bore.

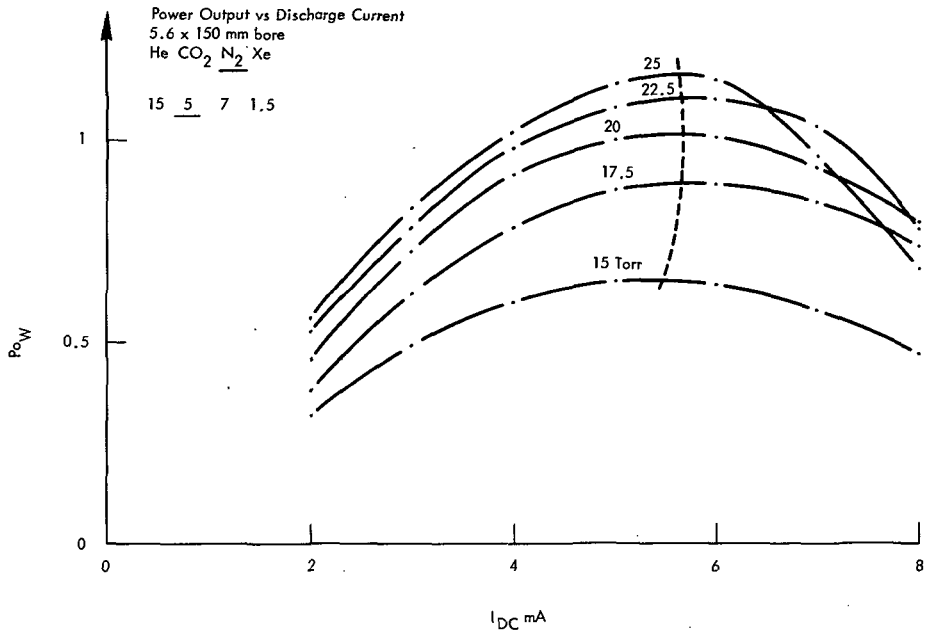


Figure 9. Power output as a function of discharge current [$P_o(W)$ versus I_{DC} (mA)] for a 150-mm length laser tube with a 5.6-mm bore.

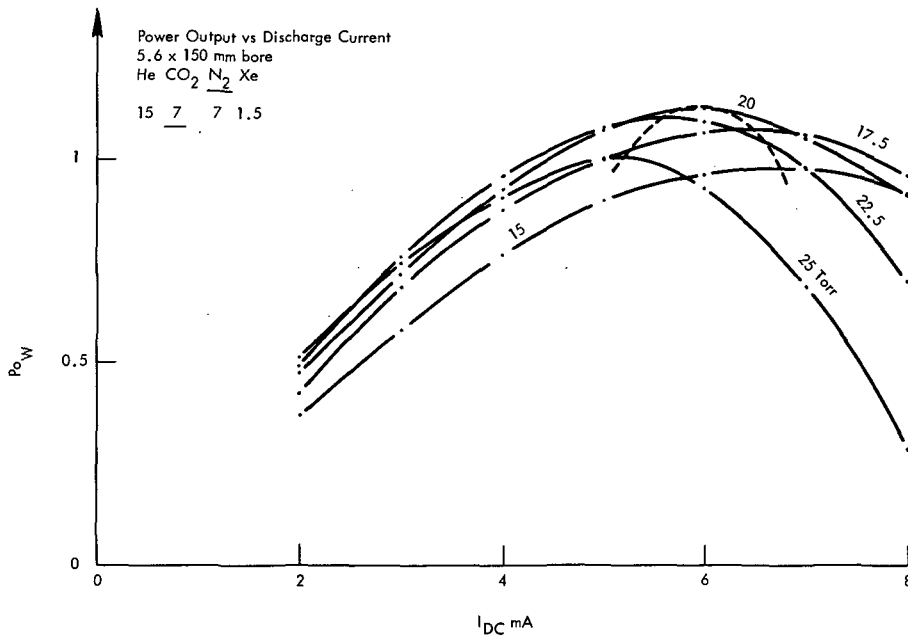


Figure 10. Power output as a function of discharge current [$P_o(W)$ versus I_{DC} (mA)] for a 150-mm length laser tube with a 5.6-mm bore.

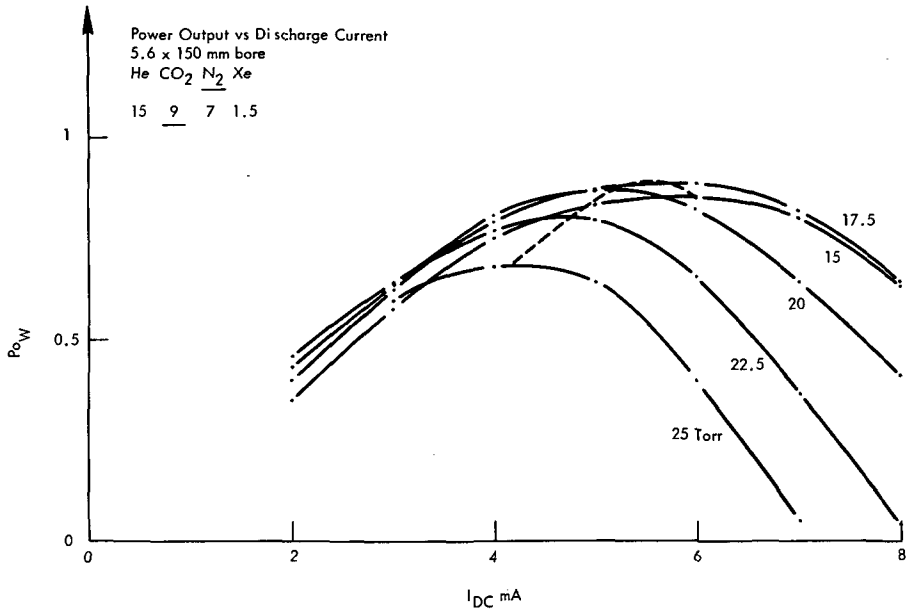


Figure 11. Power output as a function of discharge current [$P_o(W)$ versus I_{DC} (mA)] for a 150-mm length laser tube with a 5.6-mm bore.

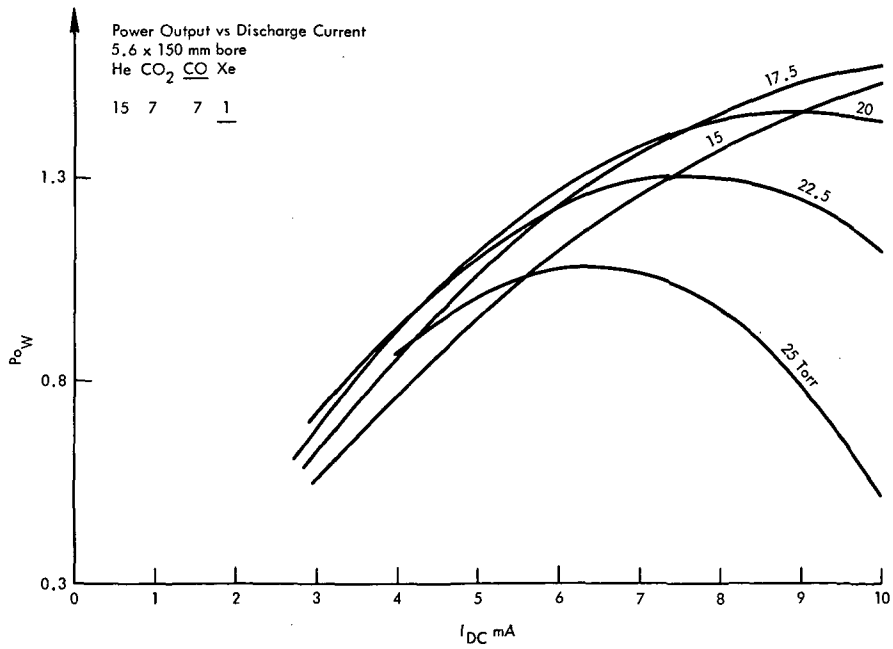


Figure 12. Power output as a function of discharge current [$P_o(W)$ versus I_{DC} (mA)] for a 150-mm length laser tube with a 5.6-mm bore.

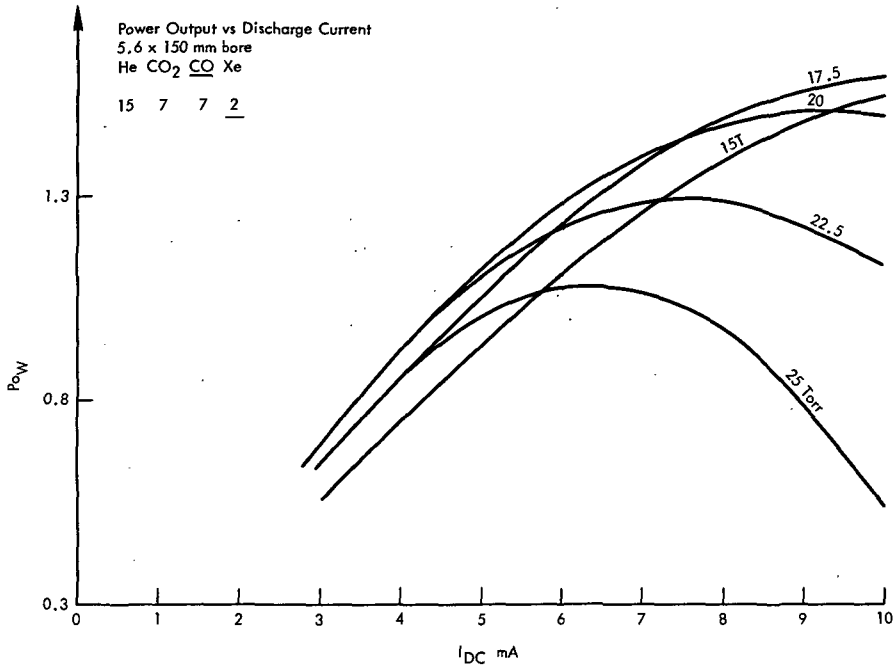


Figure 13. Power output as a function of discharge current [Po(W) versus I_{DC} (mA)] for a 150-mm length laser tube with a 5.6-mm bore.

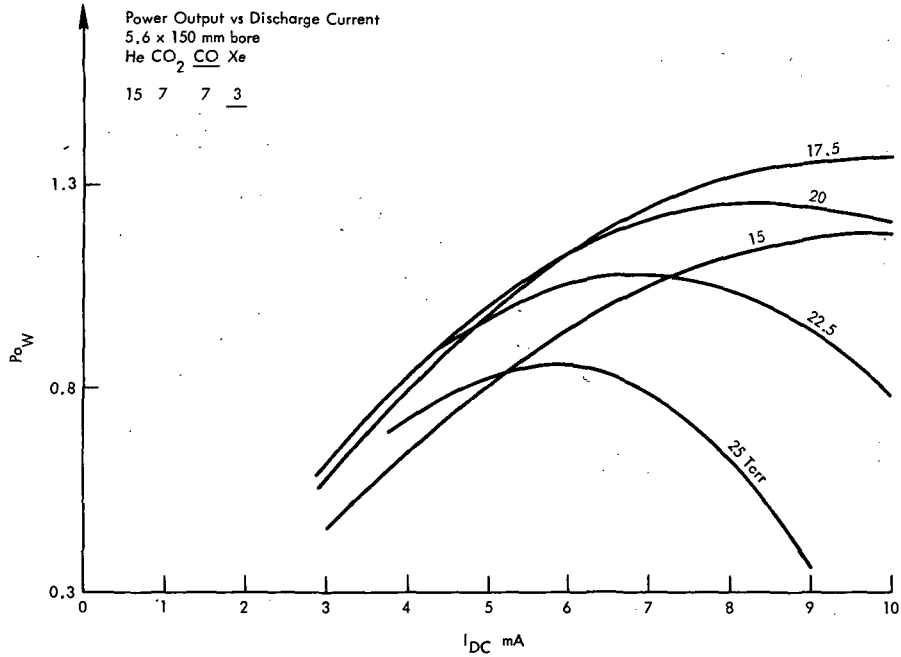


Figure 14. Power output as a function of discharge current [Po(W) versus I_{DC} (mA)] for a 150-mm length laser tube with a 5.6-mm bore.

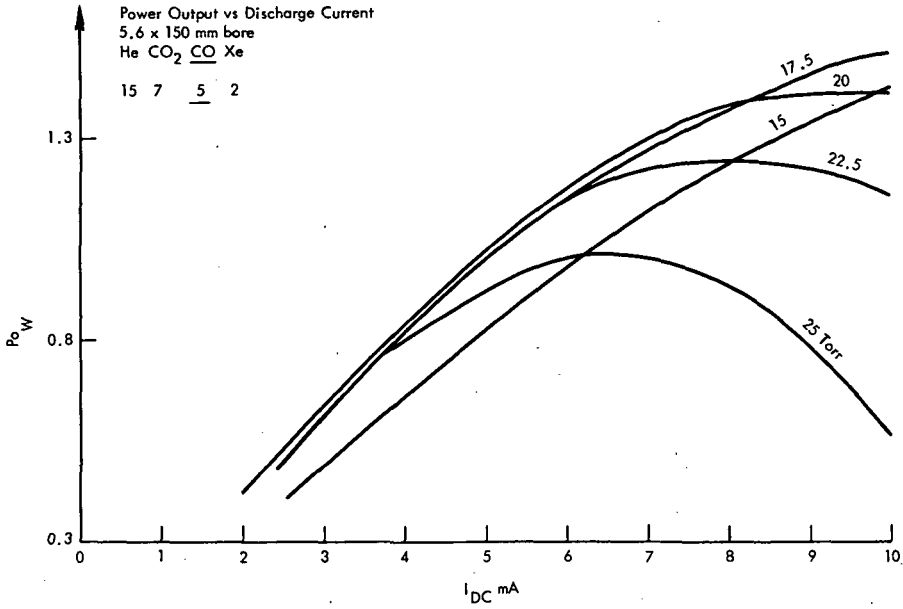


Figure 15. Power output as a function of discharge current [P_o (W) versus I_{DC} (mA)] for a 150-mm length laser tube with a 5.6-mm bore.

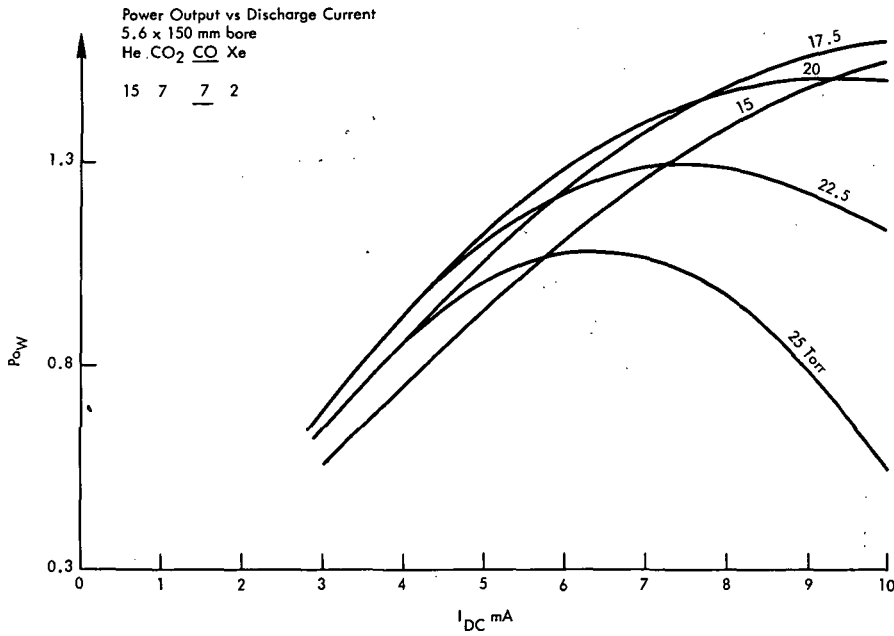


Figure 16. Power output as a function of discharge current [P_o (W) versus I_{DC} (mA)] for a 150-mm length laser tube with a 5.6-mm bore.

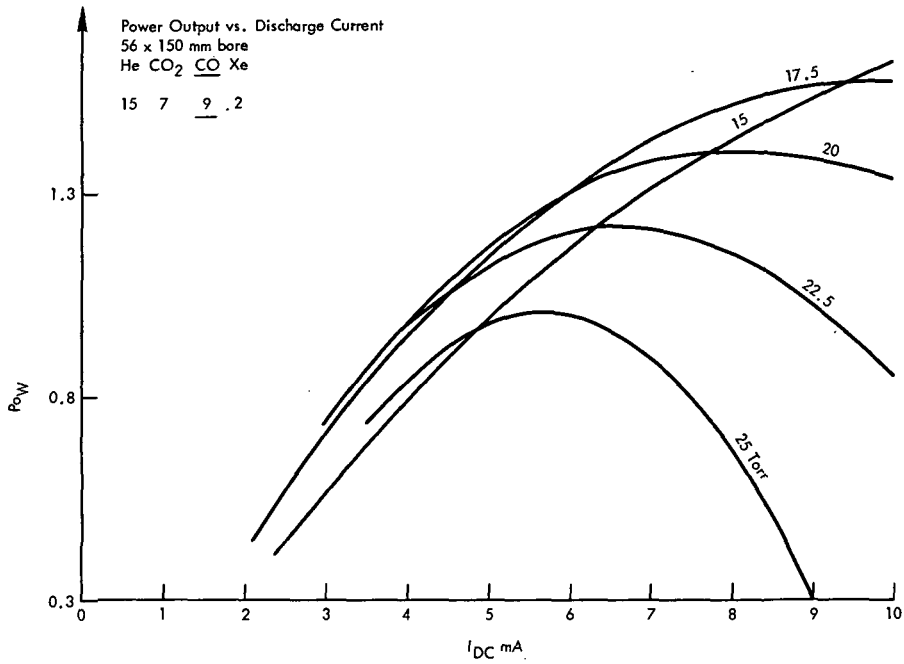


Figure 17. Power output as a function of discharge current [P_o (W) versus I_{DC} (mA)] for a 150-mm length laser tube with a 5.6-mm bore.

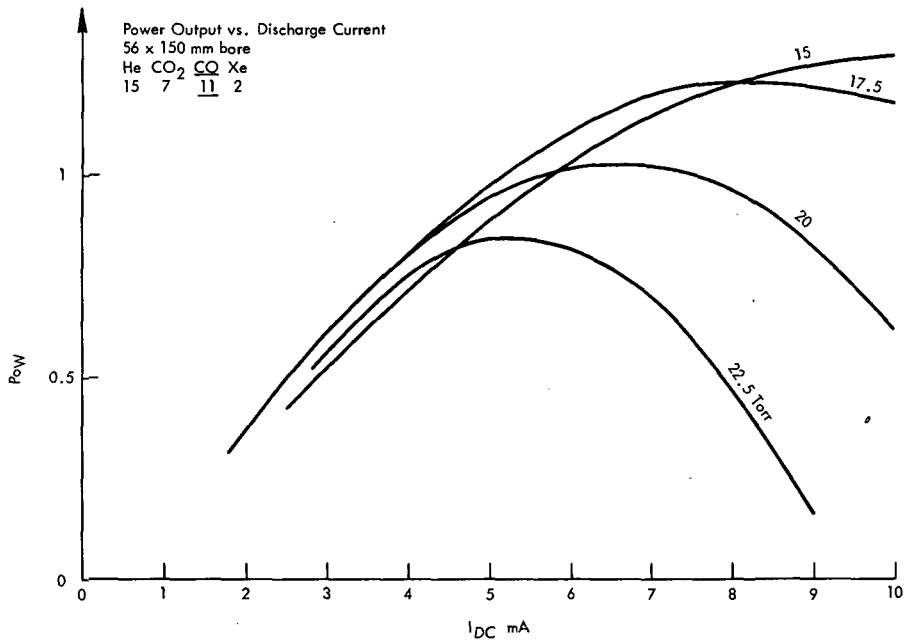


Figure 18. Power output as a function of discharge current [P_o (W) versus I_{DC} (mA)] for a 150-mm length laser tube with a 5.6-mm bore.

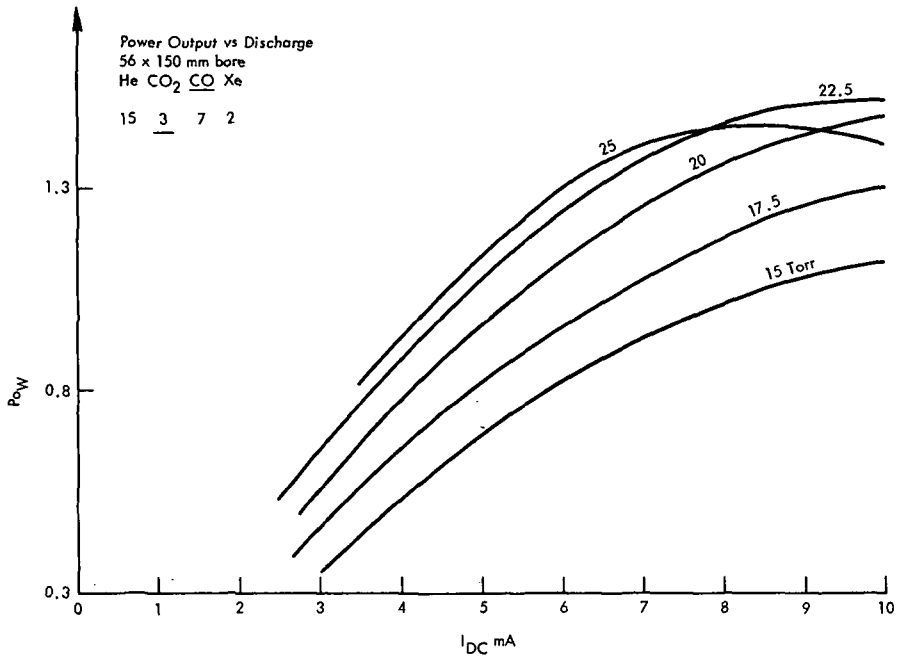


Figure 19. Power output as a function of discharge current [Po(W) versus I_{DC} (mA)] for a 150-mm length laser tube with a 5.6-mm bore.

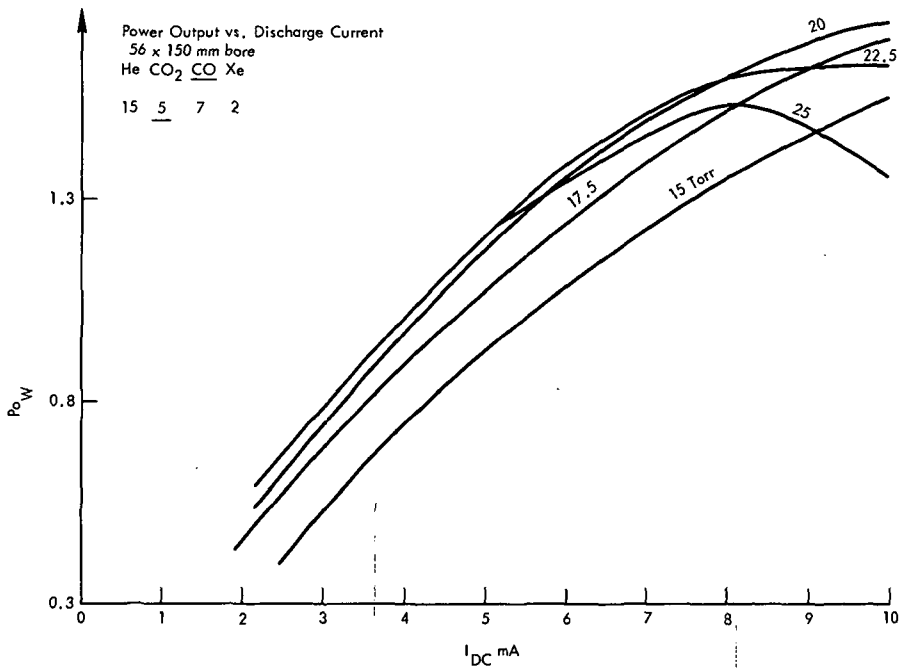


Figure 20. Power output as a function of discharge current [Po(W) versus I_{DC} (mA)] for a 150-mm length laser tube with a 5.6-mm bore.

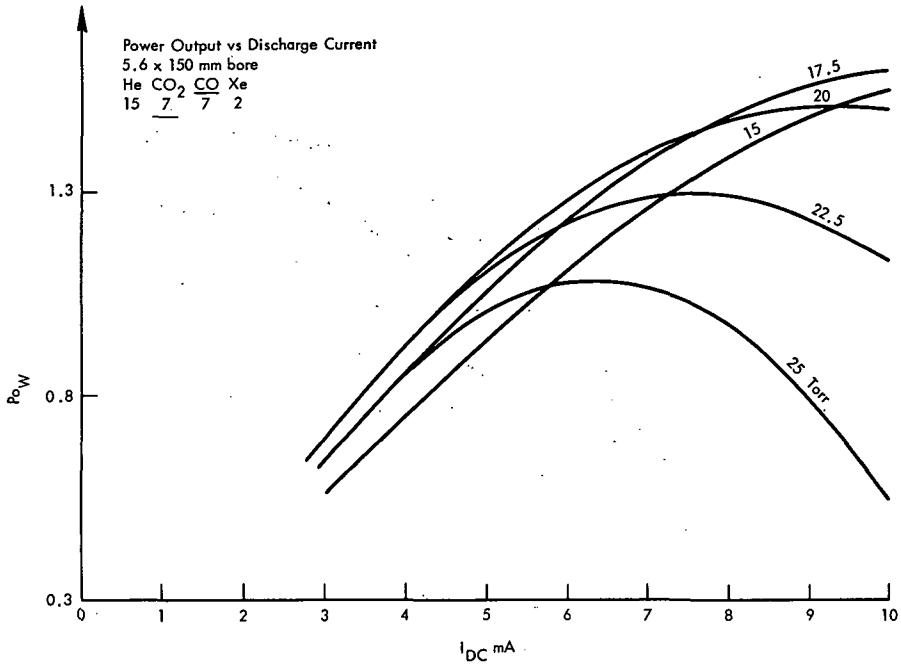


Figure 21. Power output as a function of discharge current [Po(W) versus I_{DC} (mA)] for a 150-mm length laser tube with a 5.6-mm bore.

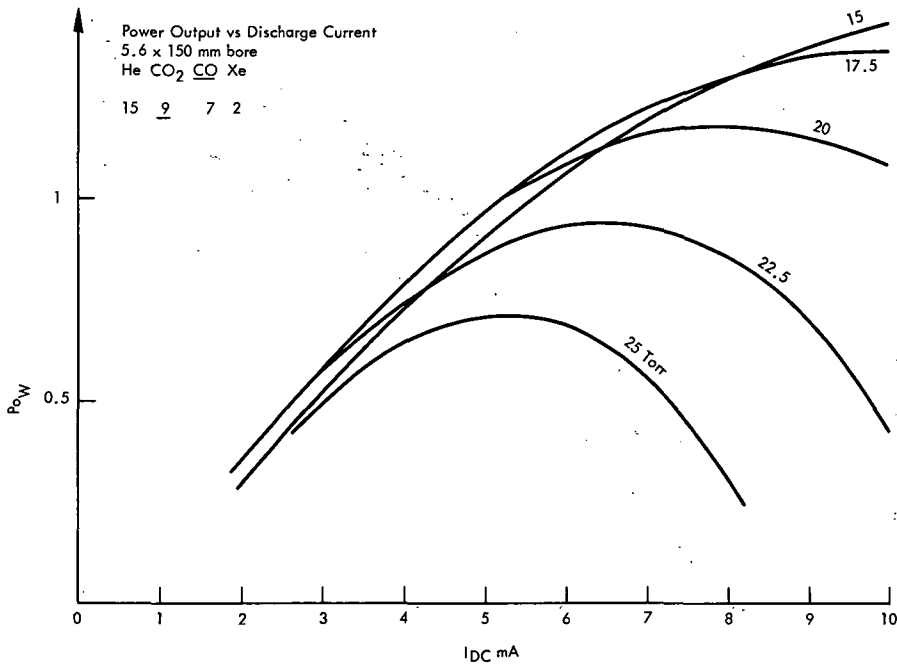


Figure 22. Power output as a function of discharge current [Po(W) versus I_{DC} (mA)] for a 150-mm length laser tube with a 5.6-mm bore.

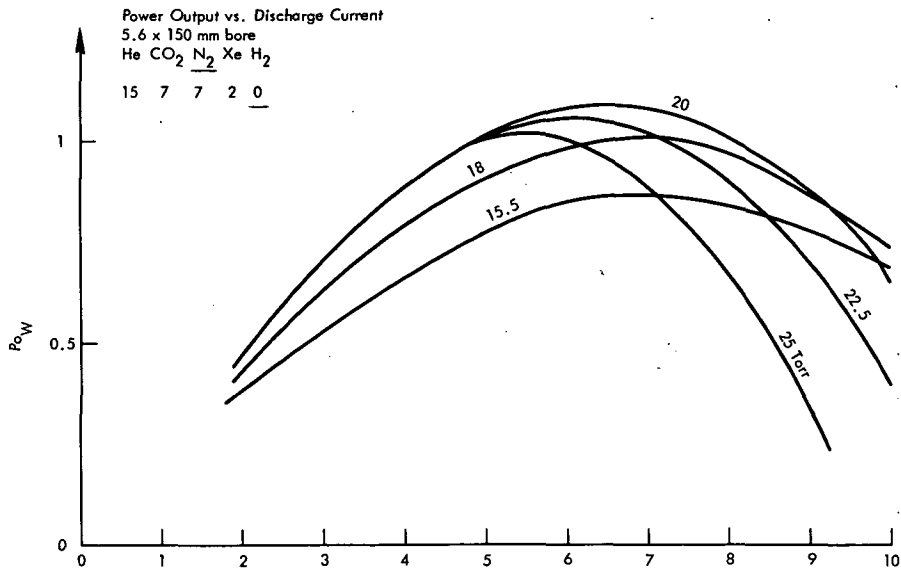


Figure 23. Power output as a function of discharge current [$P_o(W)$ versus I_{DC} (mA)] for a 150-mm length laser tube with a 5.6-mm bore.

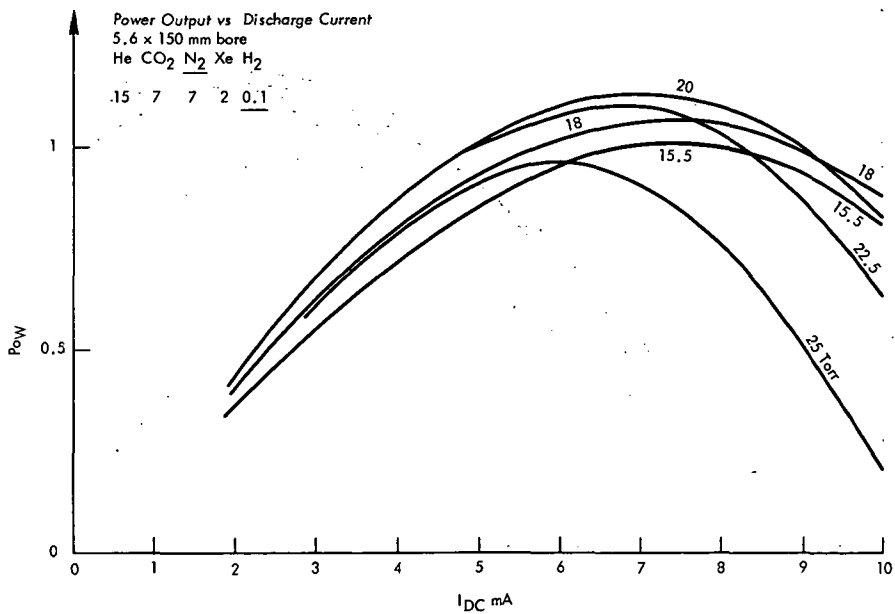


Figure 24. Power output as a function of discharge current [$P_o(W)$ versus I_{DC} (mA)] for a 150-mm length laser tube with a 5.6-mm bore.

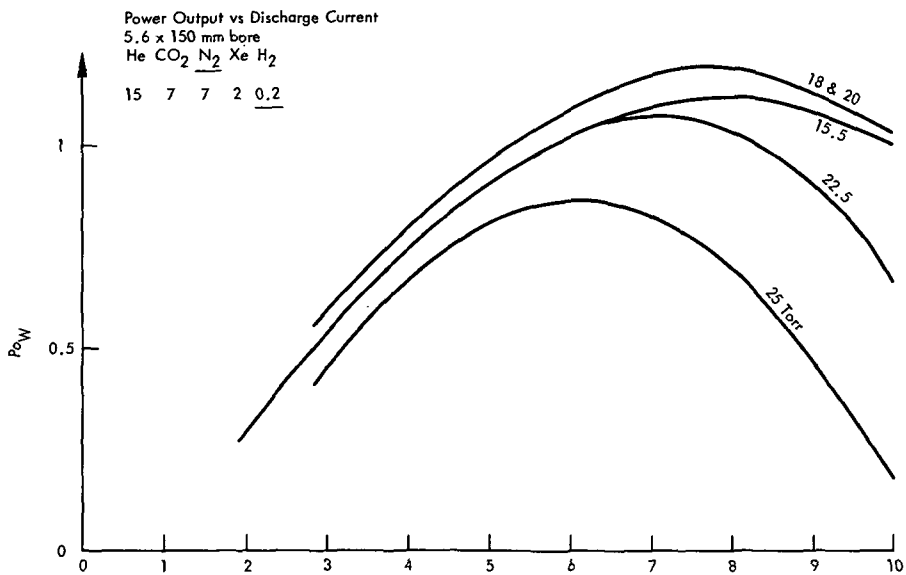


Figure 25. Power output as a function of discharge current [Po(W) versus I_{DC} (mA)] for a 150-mm length laser tube with a 5.6-mm bore.

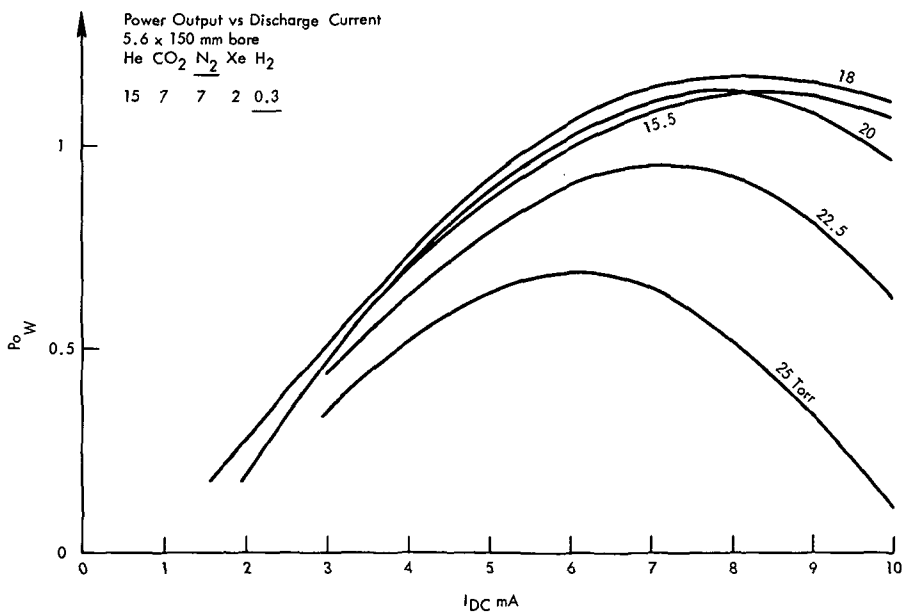


Figure 26. Power output as a function of discharge current [Po(W) versus I_{DC} (mA)] for a 150-mm length laser tube with a 5.6-mm bore.

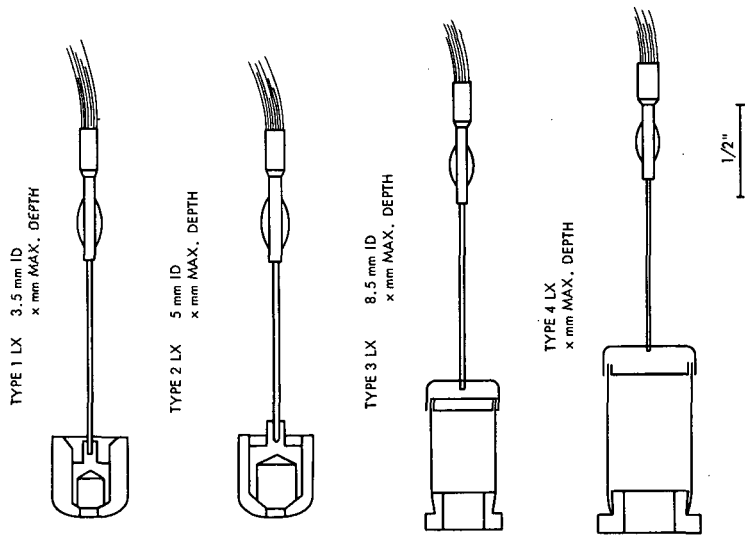


Figure 27. Cathode types.

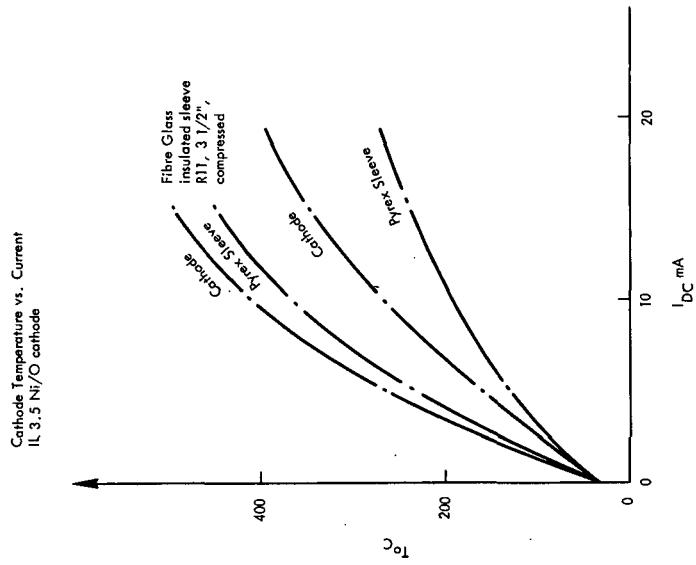


Figure 28. Cathode current [$T(^{\circ}C)$] versus current (I_{DC}).

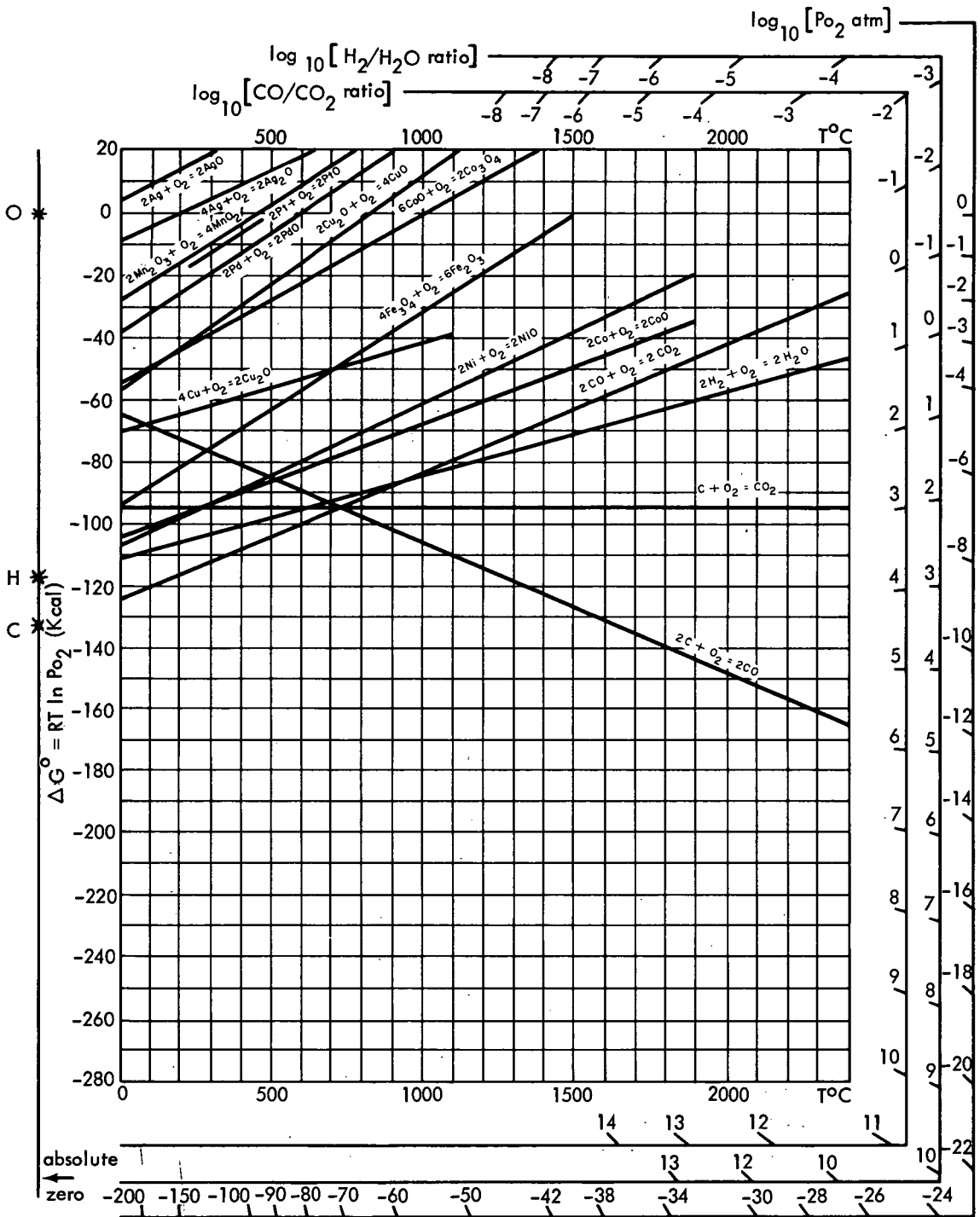


Figure 29. Standard free energy of formation of oxides as a function of temperature.

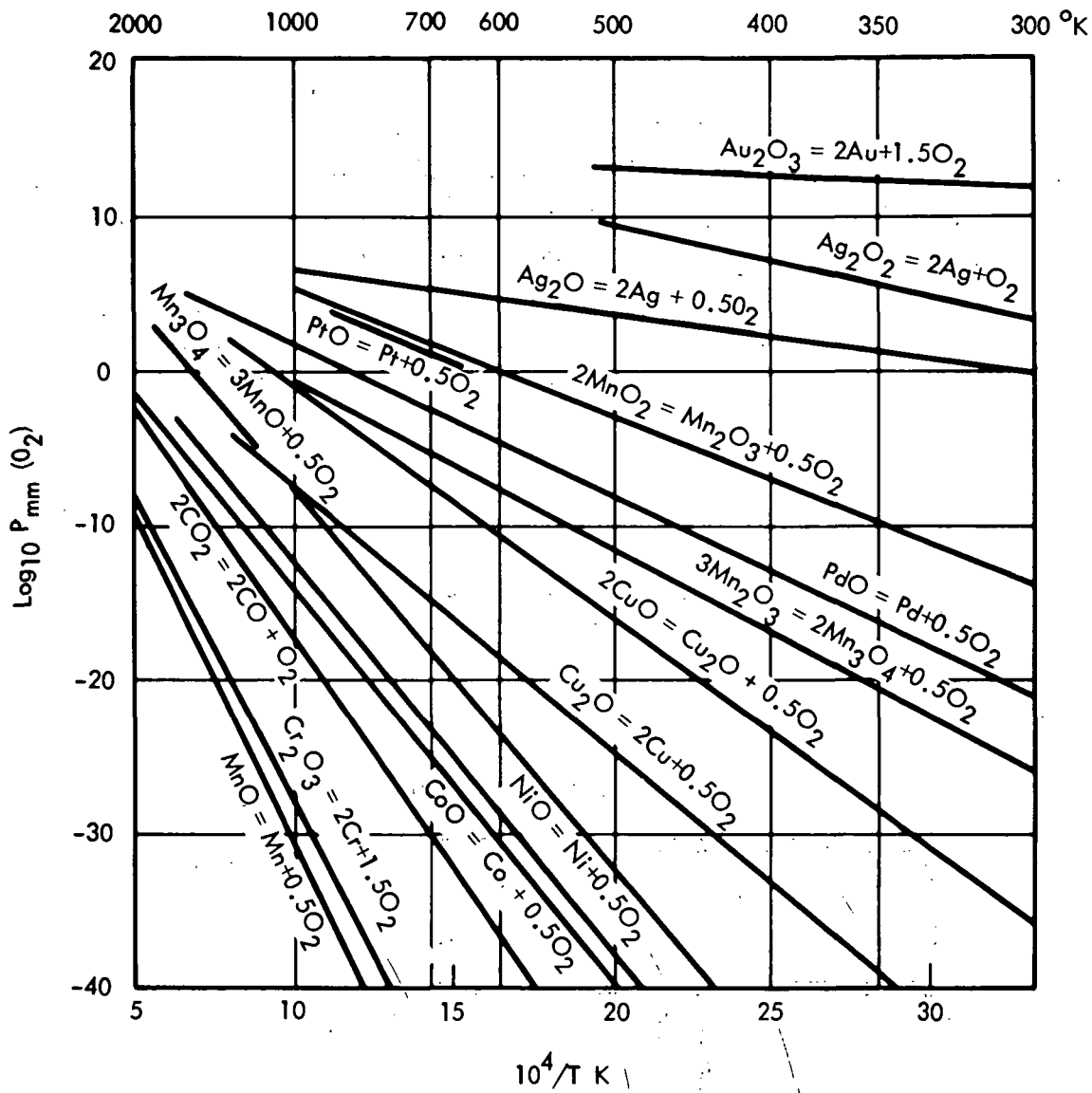


Figure 30. Dissociation pressure of oxides as a function of temperature.

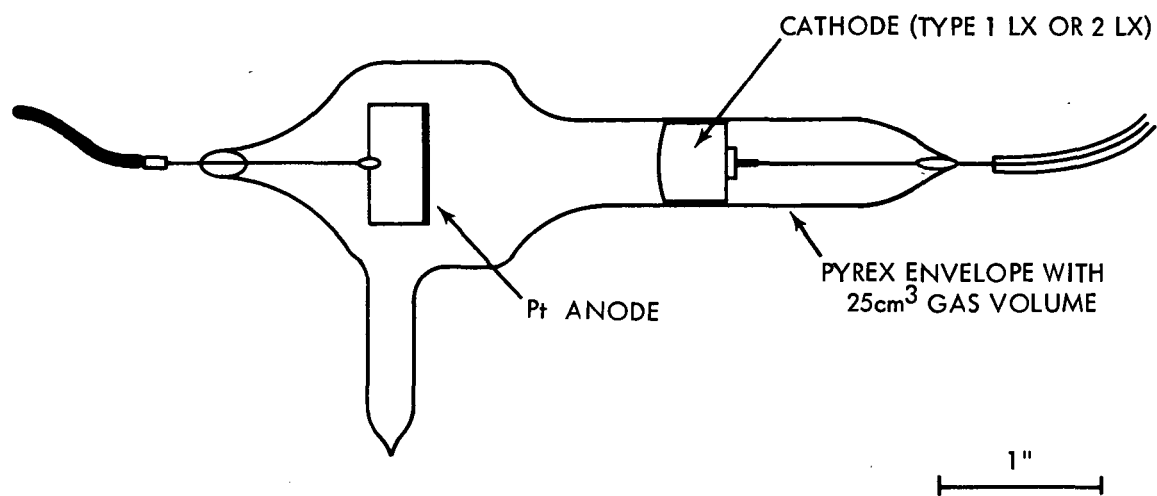


Figure 31. Discharge tube.

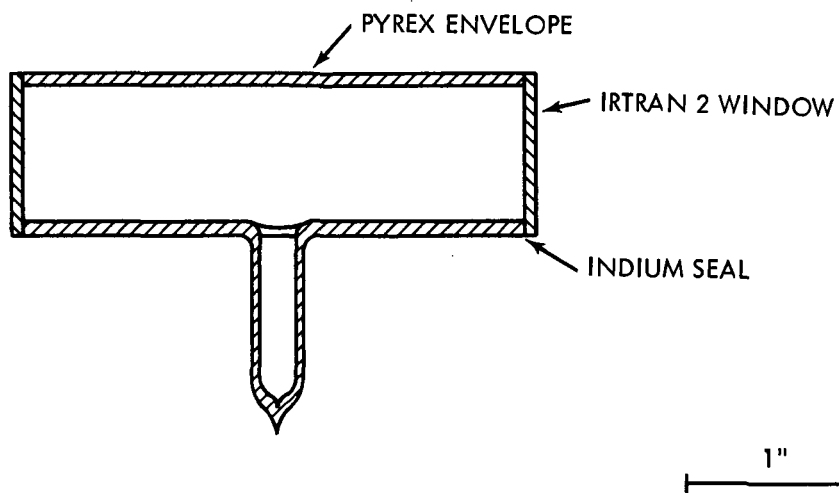


Figure 32. Infrared absorption cell.

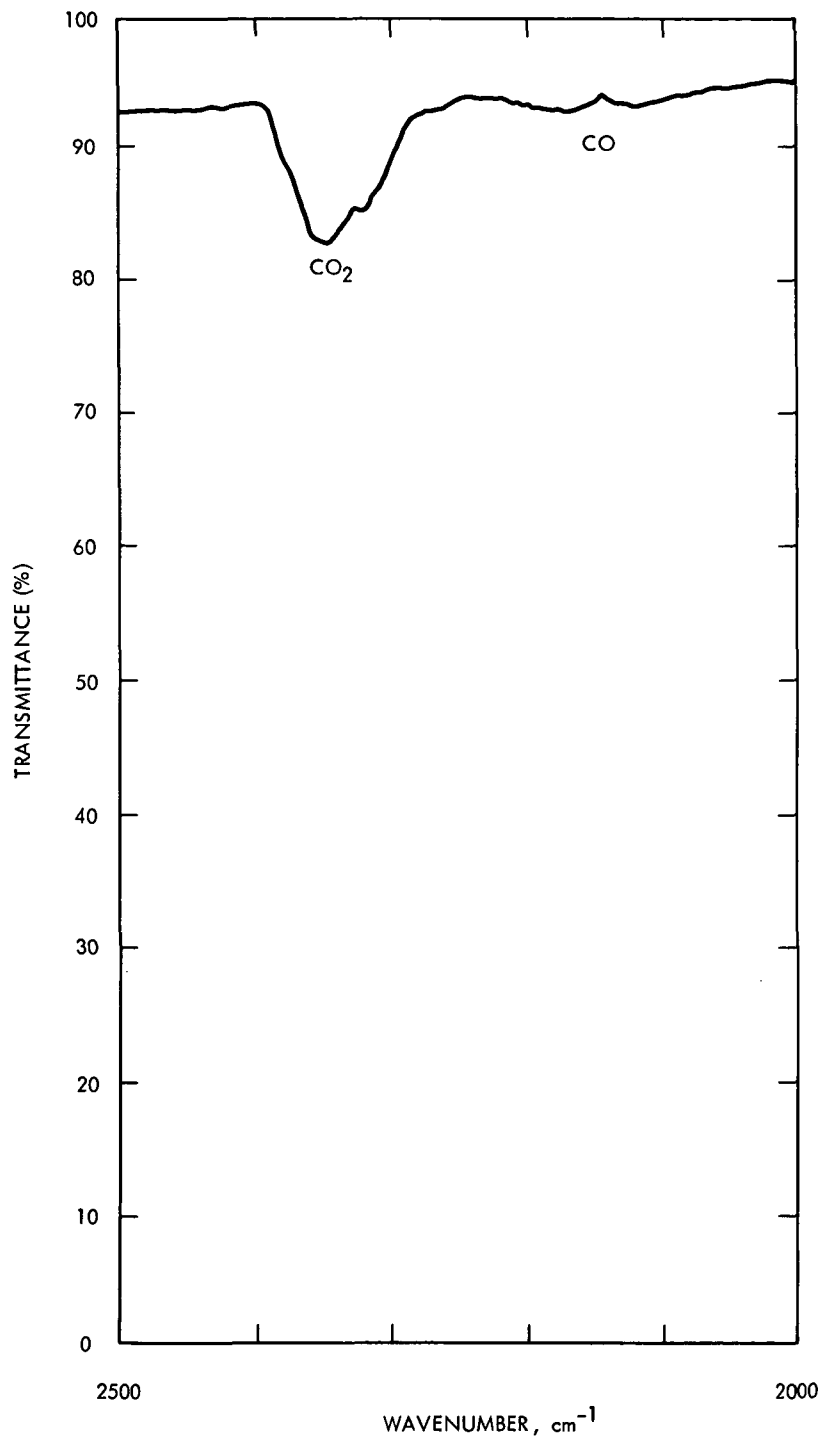


Figure 33. Infrared spectrum of CO₂ and CO in a gas mix of 20.1 torr total pressure (4.7 CO₂; 4.7 CO; 0.7 Xe; and 10 torr He) in a 7.8 cm path length cell employing a Digilab FTS-14 with equivalent slit width of 8 cm⁻⁷.

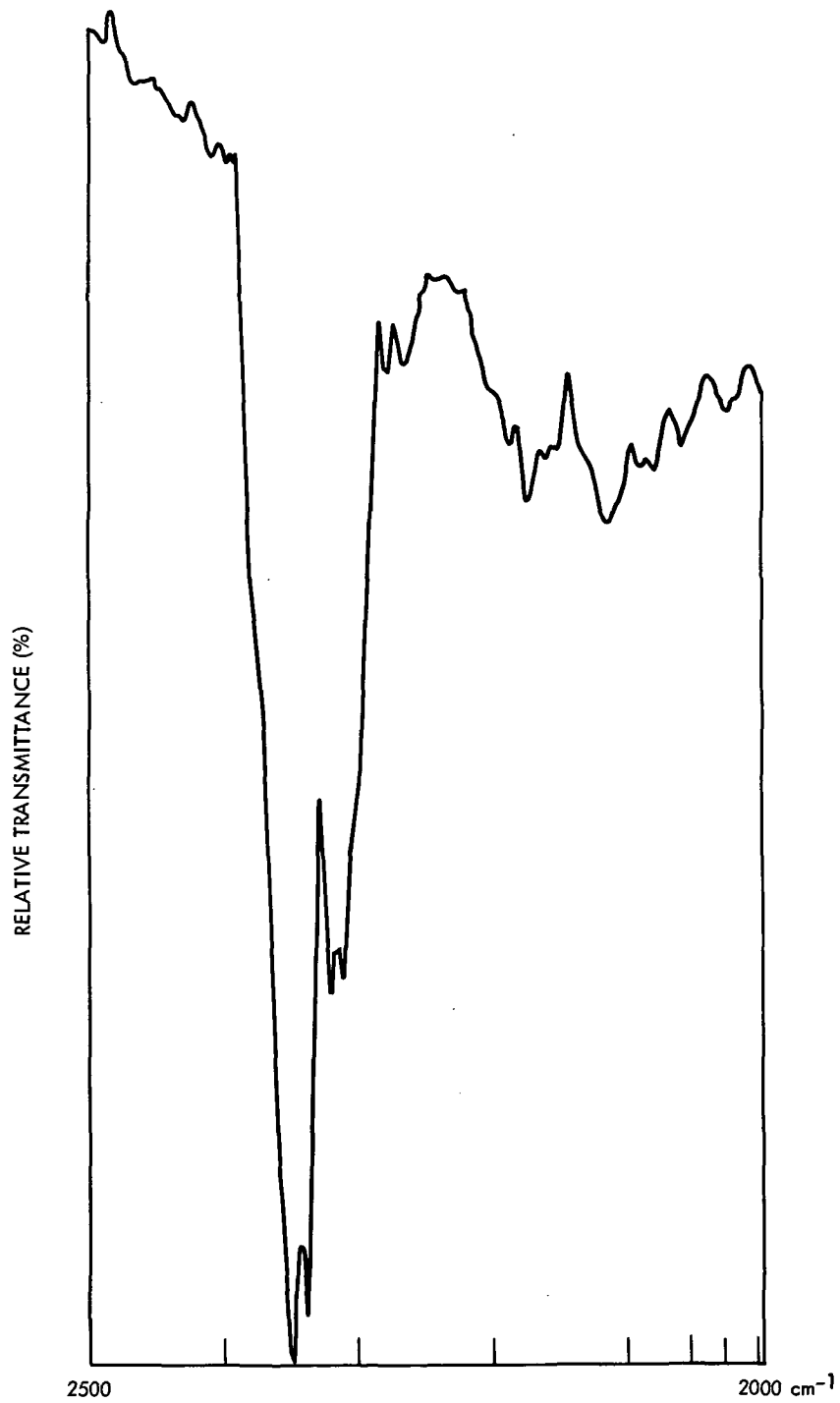


Figure 34. Infrared absorption spectrum of CO₂ and CO (expanded scale).

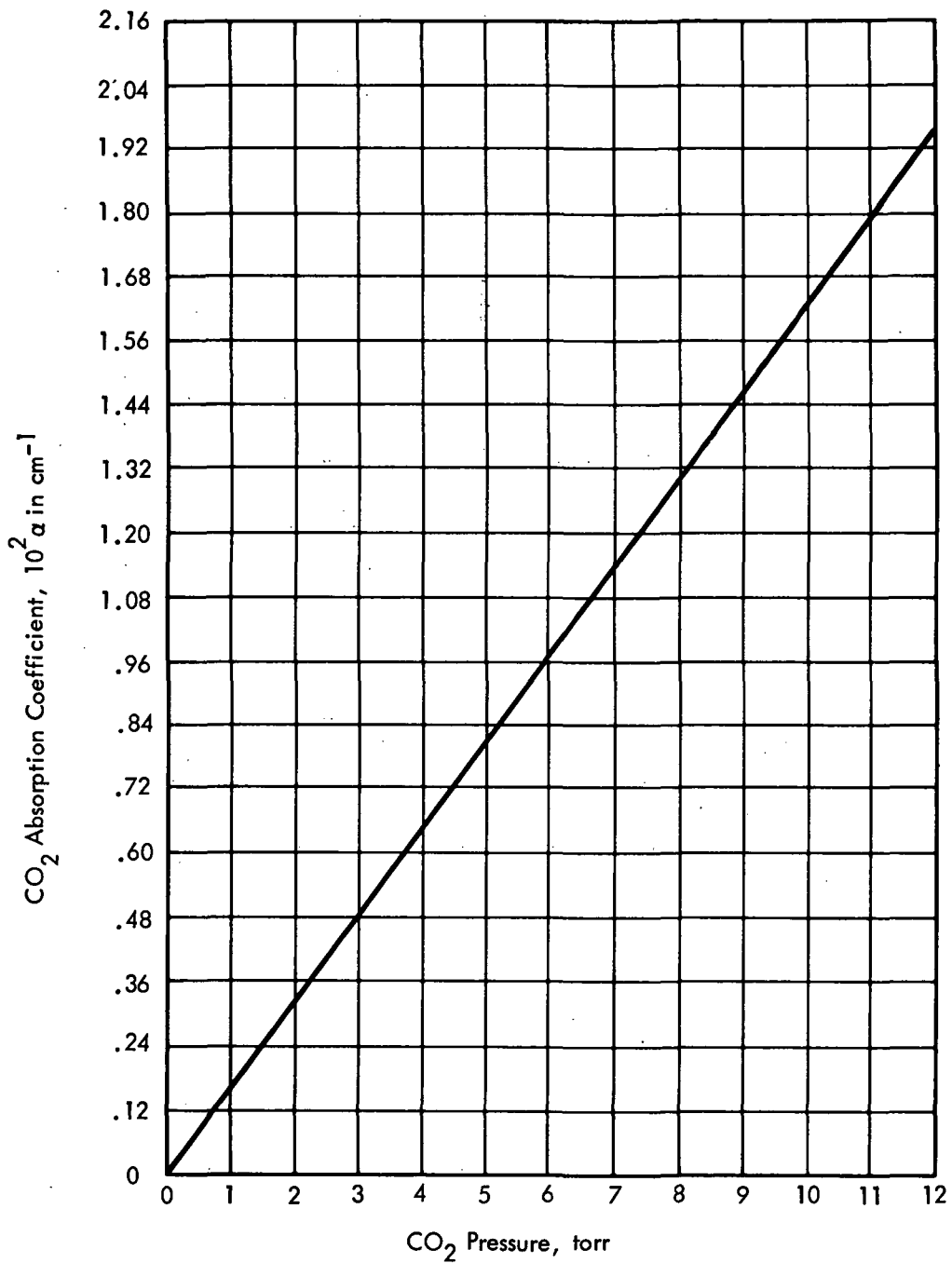


Figure 35. Plot of absorption coefficient, α , of pure CO₂ versus CO₂ pressure for $\alpha = [\ln(I_0/I)]/x$ measured at $\nu = 2355 \text{ cm}^{-1}$, $x = 8 \text{ cm}$ and 75° F temperature, and 8 cm^{-1} equivalent slit width.

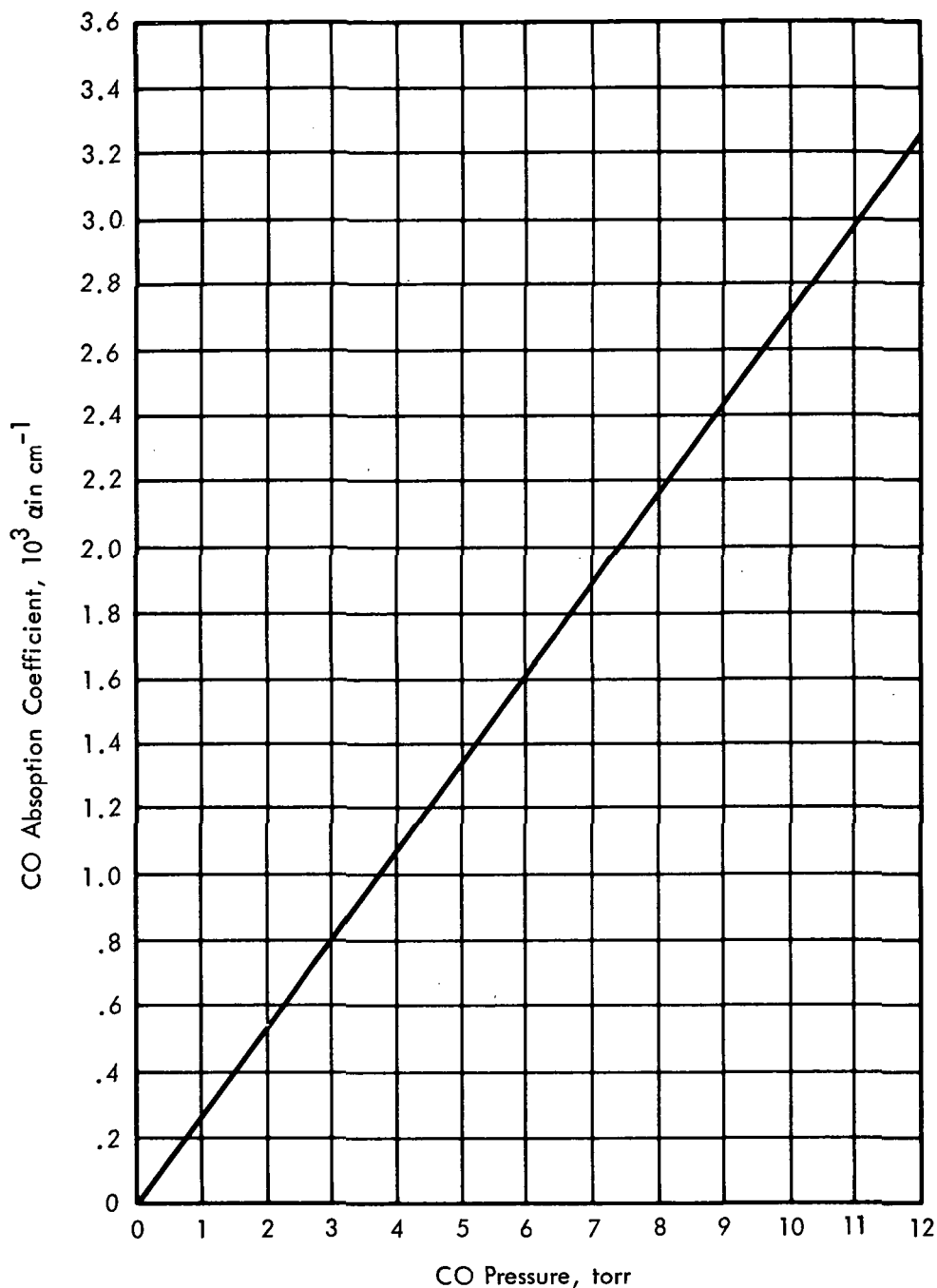


Figure 36. Plot of absorption coefficient, α , of pure CO versus CO pressure for $\alpha = [\ln(I_0/I)]/x$ measured at $\bar{\nu} = 2175 \text{ cm}^{-1}$, $x = 8 \text{ cm}$ and 75° F temperature, and 8 cm^{-1} equivalent slit width.

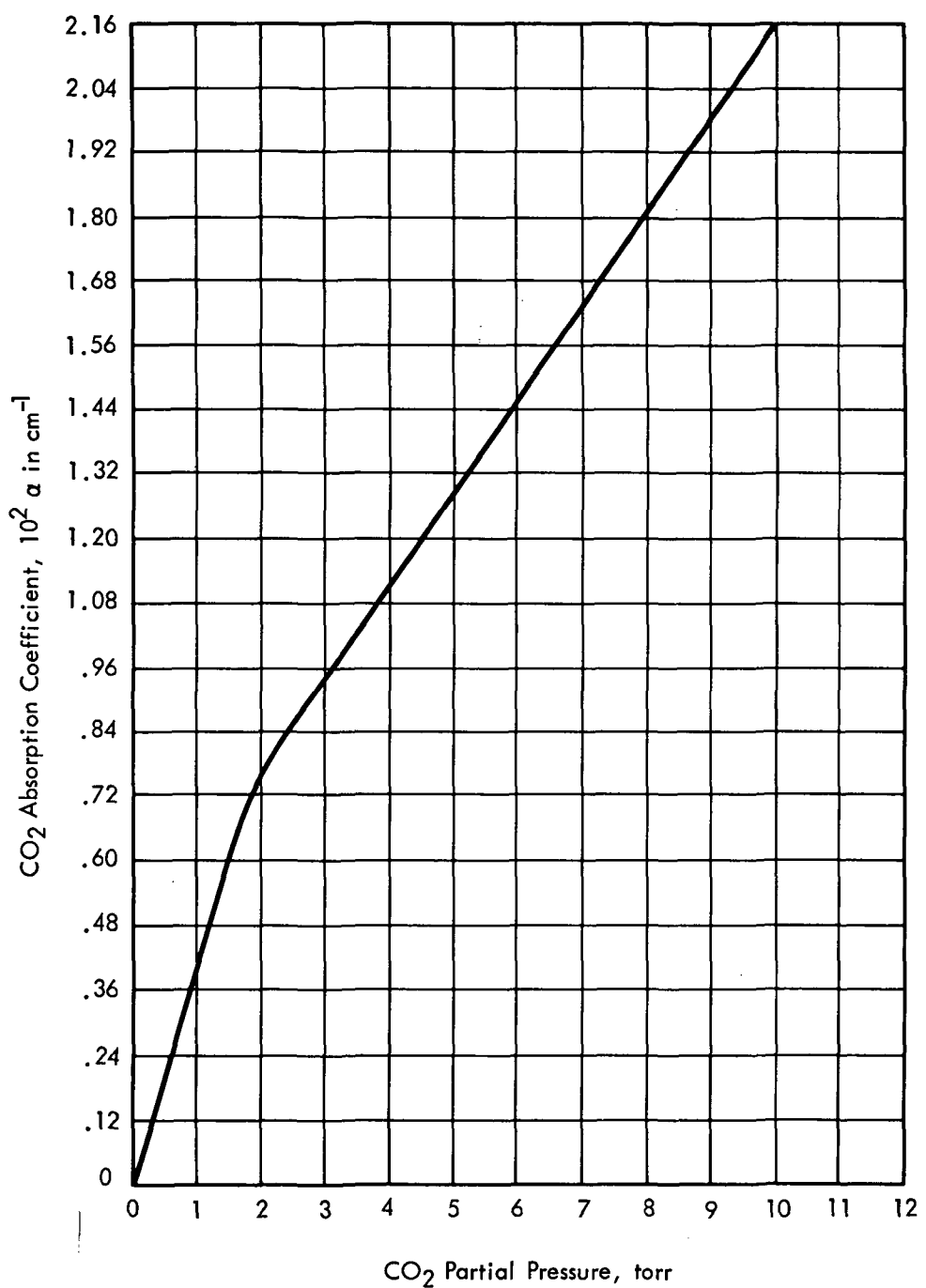


Figure 37. Plot of absorption coefficient, α , of CO_2 versus partial pressure, P , for a gas mixture of 20 torr total pressure (P torr CO_2 , $10-P$ torr CO , 9.4 torr He , 0.6 torr Xe) and $\alpha = [\ln(I_0/I)]/x$ measured at $\bar{\nu} = 2355 \text{ cm}^{-1}$, $x = 8 \text{ cm}$ and 75° F , and 8 cm^{-1} equivalent slit width.

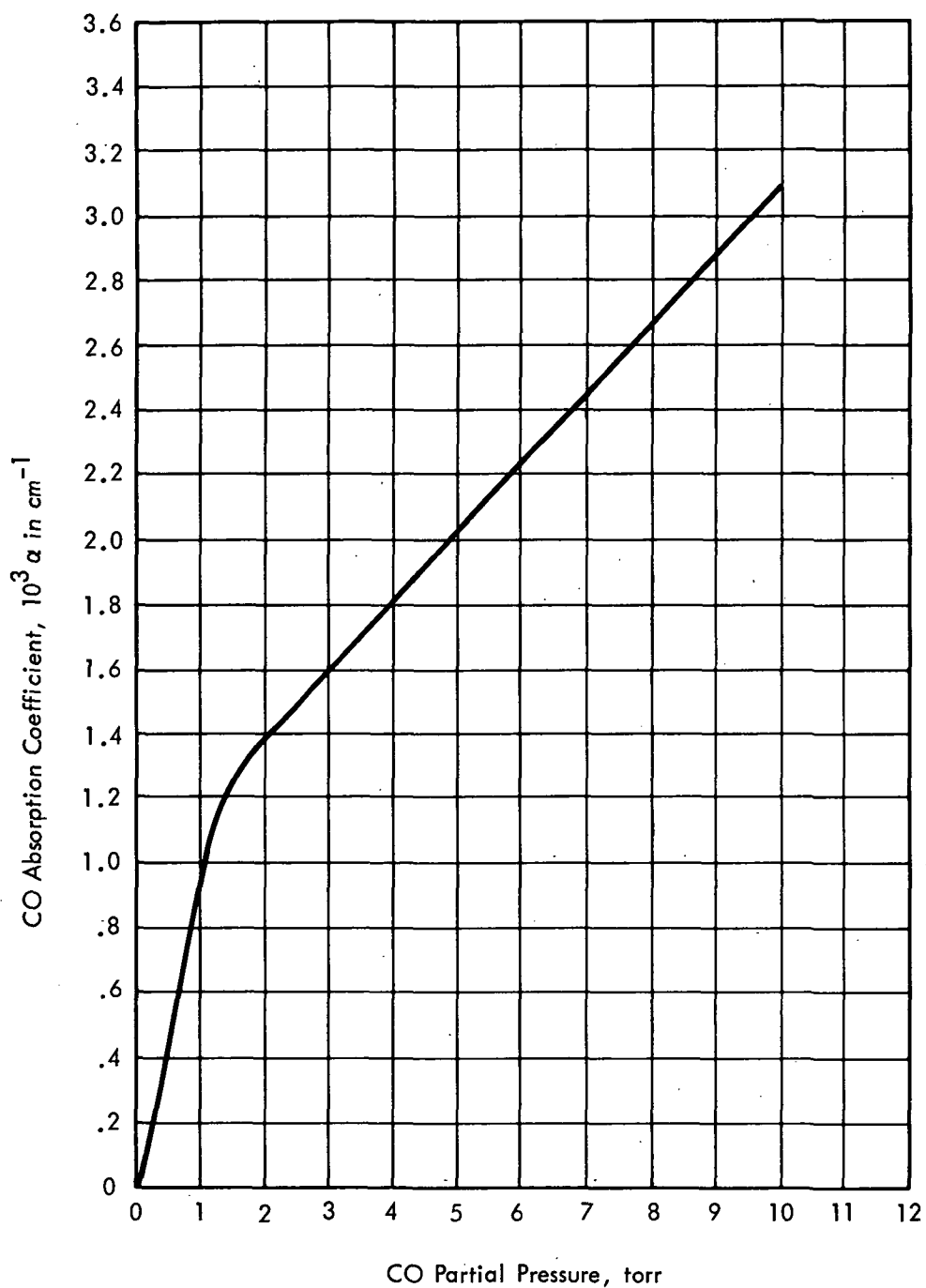


Figure 38. Plot of absorption coefficient, α , of CO versus CO partial pressure, P , for a gas mixture of 20 torr total pressure (P torr CO, $10-P$ torr CO_2 , 9.4 torr He, 0.6 torr Xe) and $\alpha = [\ln(I_0/I)]/x$ measured at $\bar{\nu} = 2175 \text{ cm}^{-1}$, $x = 8 \text{ cm}$ and 75° F , and 8 cm^{-1} equivalent slit width.

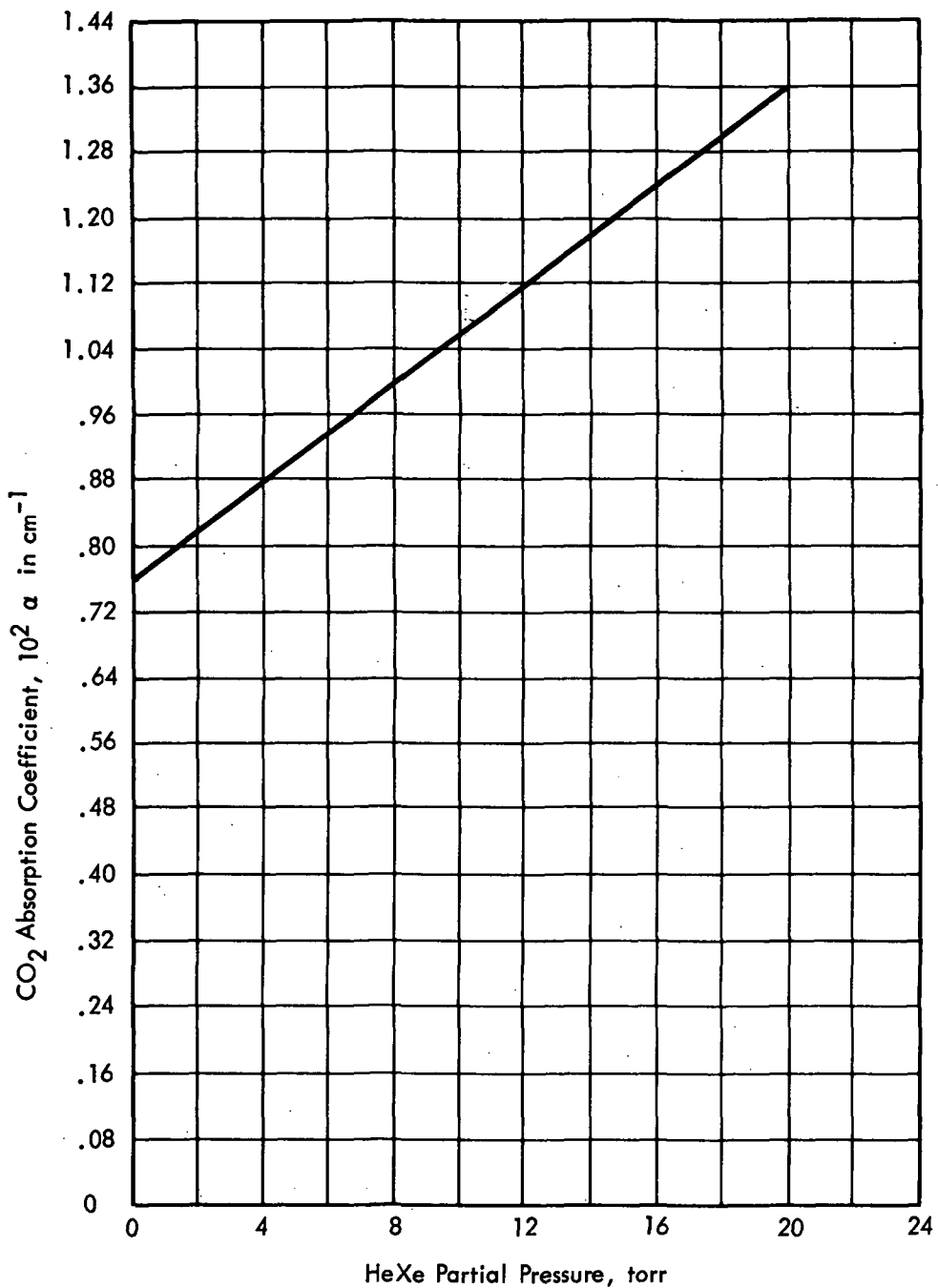


Figure 39. Plot of absorption coefficient, α , of 4.65 torr CO₂ versus HeXe partial pressure, P, for a gas mixture of P + 4.65 torr total pressure and $\alpha = [\ln(I_0/I)]/x$ measured at $\nu = 2355 \text{ cm}^{-1}$, $x = 8$ and 75° F and 8 cm⁻¹ equivalent slit width.

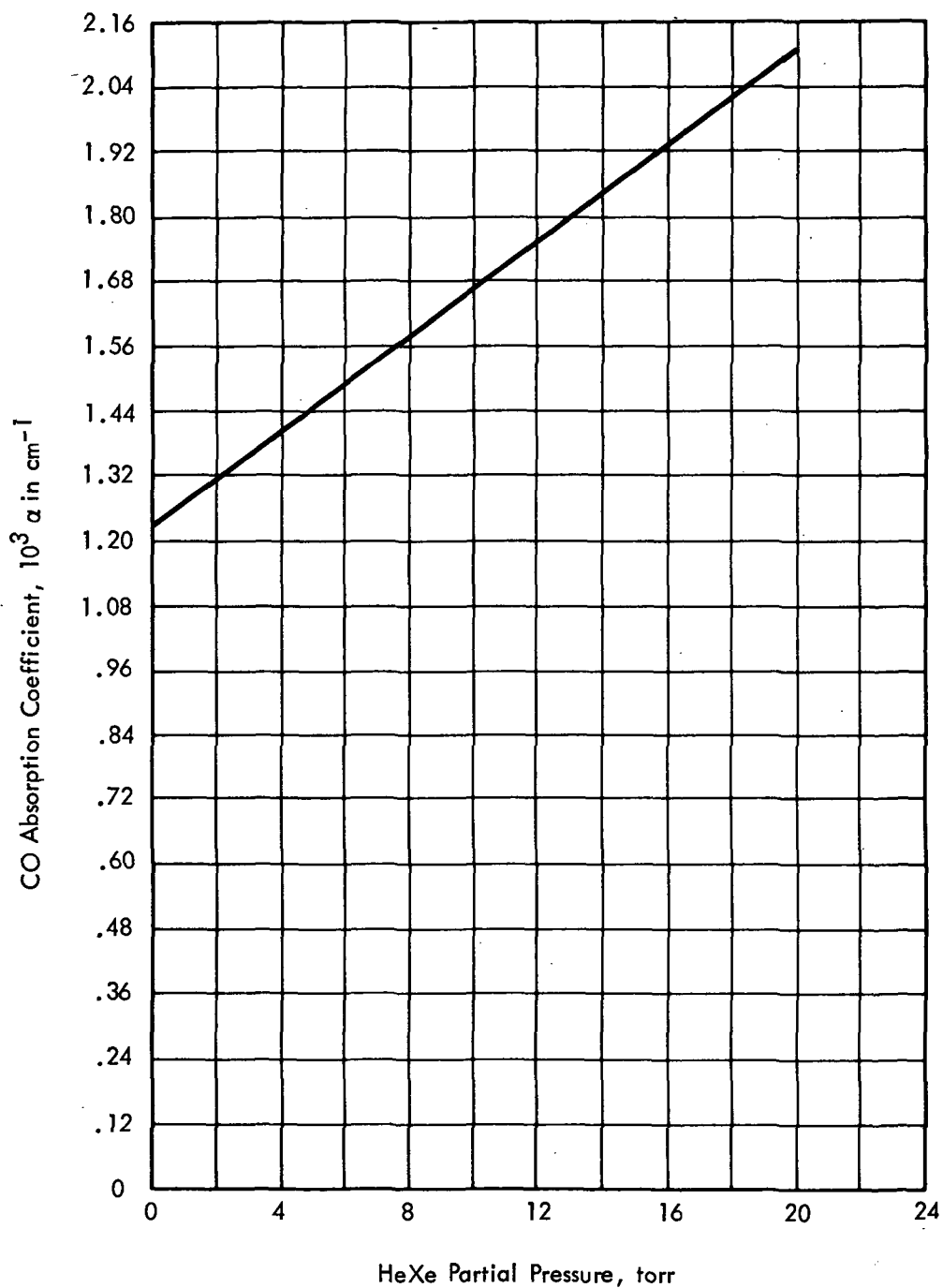


Figure 40. Plot of absorption coefficient, α , of 4.65 torr CO versus HeXe partial pressure, P , for a gas mixture of $P + 4.65$ torr total pressure and $\alpha = [\ln(I_0/I)]/x$ measured at $\nu = 2175 \text{ cm}^{-1}$, $x = 8$ and 75° F and 8 cm^{-1} equivalent slit width.

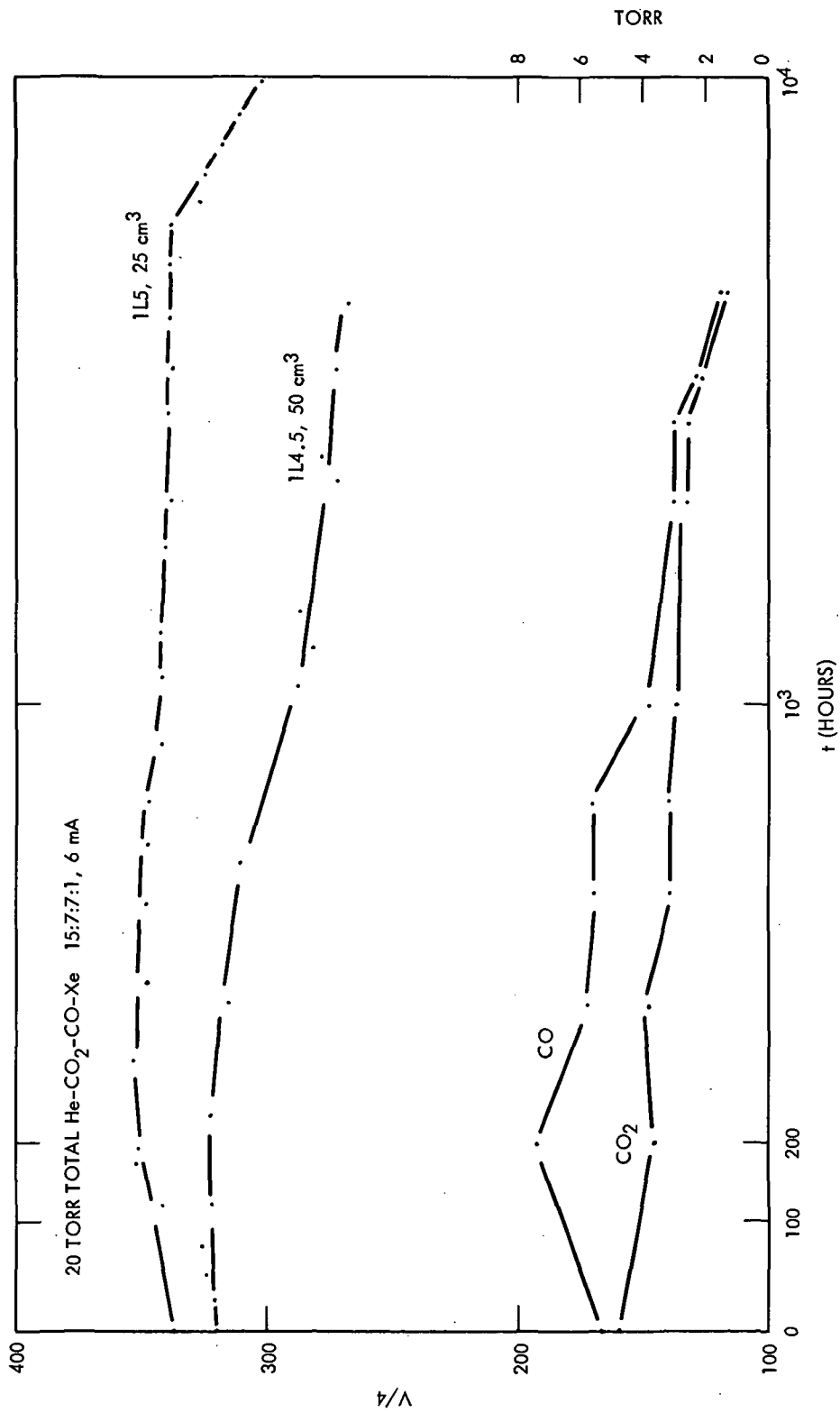


Figure 41. Silver cathodes: voltage versus operating time (upper curves) and CO₂ and CO partial pressures versus operating time (lower curves).

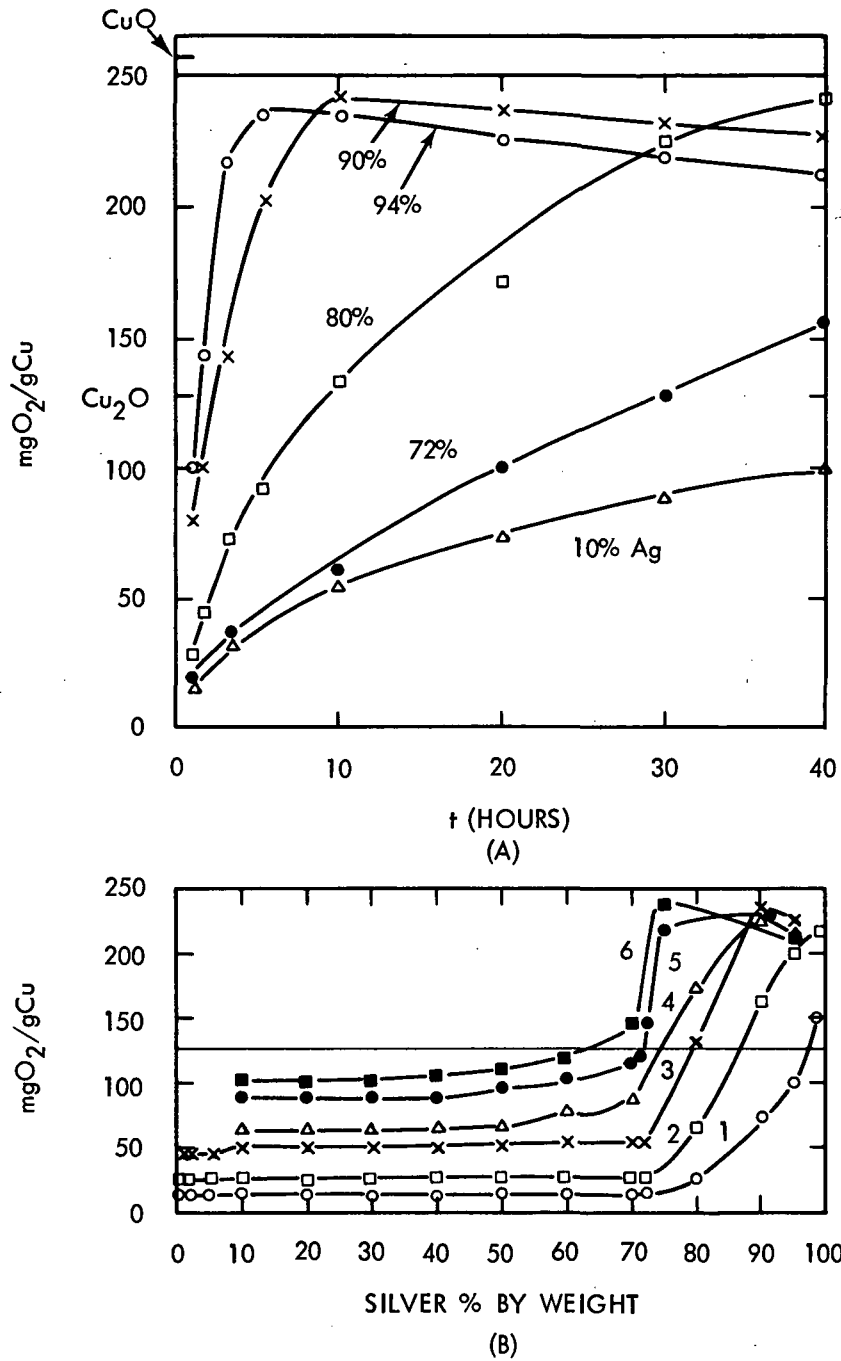


Figure 42. Silver-copper alloys: (A) internal oxidation of alloys versus time at 750°C in 1 atm of oxygen; (B) oxidation of alloys versus percent composition with curves 1 through 6 for oxidation times of 0.5, 3, 10, 20, 30, and 40 hours respectively at 750°C in 1 atm of oxygen (from E. Raub and M. Engel, *Z. F. Metalkunde*, 30, 1938, p. 83).

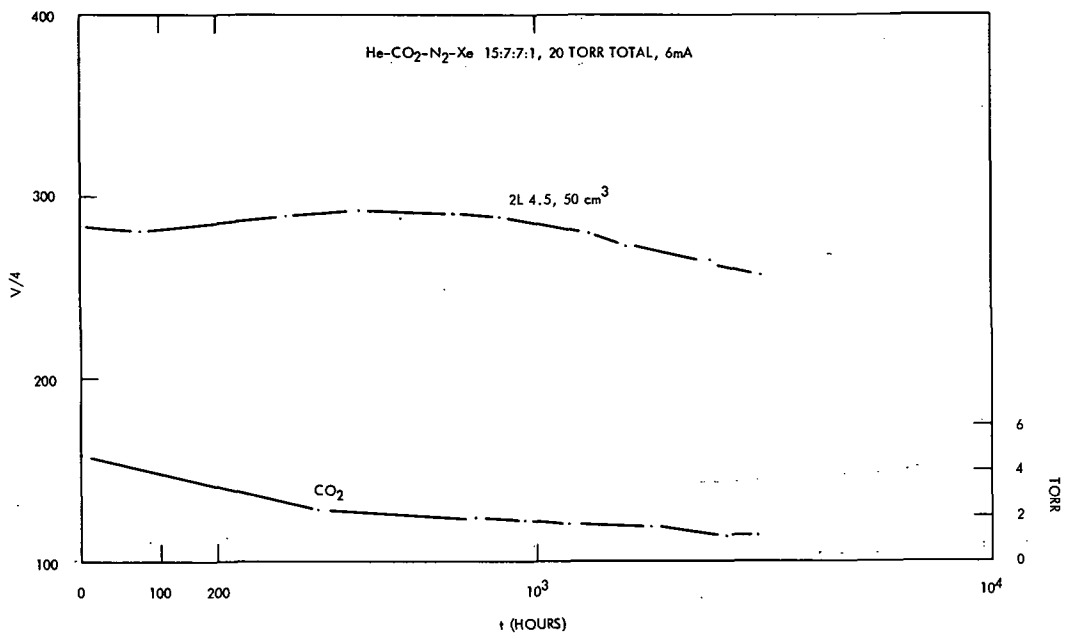


Figure 43. Silver-cadmium oxide cathode (Ag 0.8 Cd/O): voltage versus operating time (upper curve); CO₂ partial pressure versus operating time (lower curve).

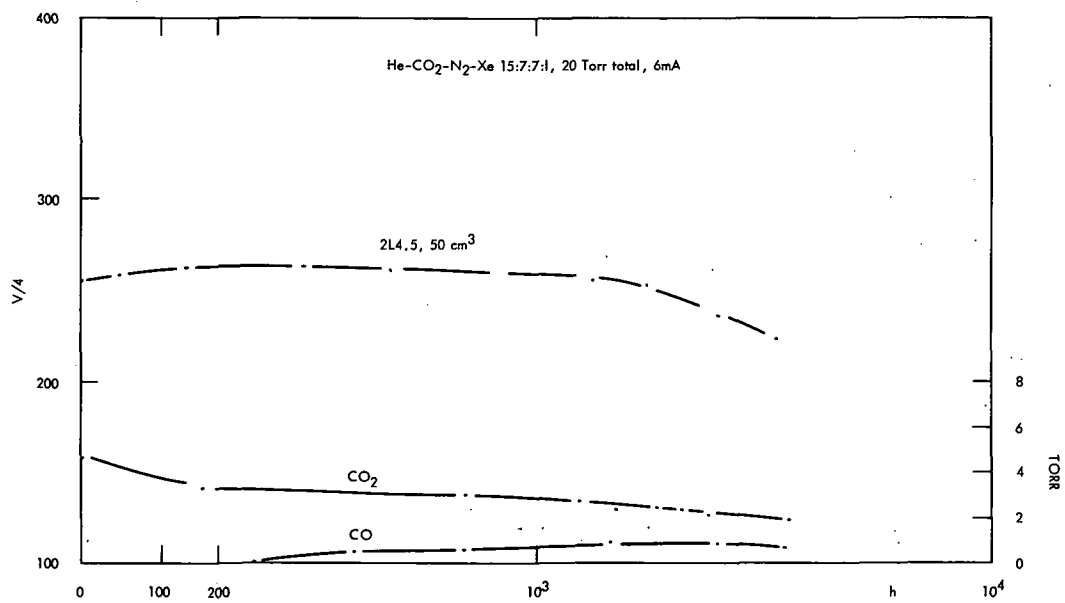


Figure 44. Silver-cadmium oxide cathode (Ag 5 Cd/O): voltage versus operating time (upper curve); CO₂ and CO partial pressures versus operating time (lower curves).

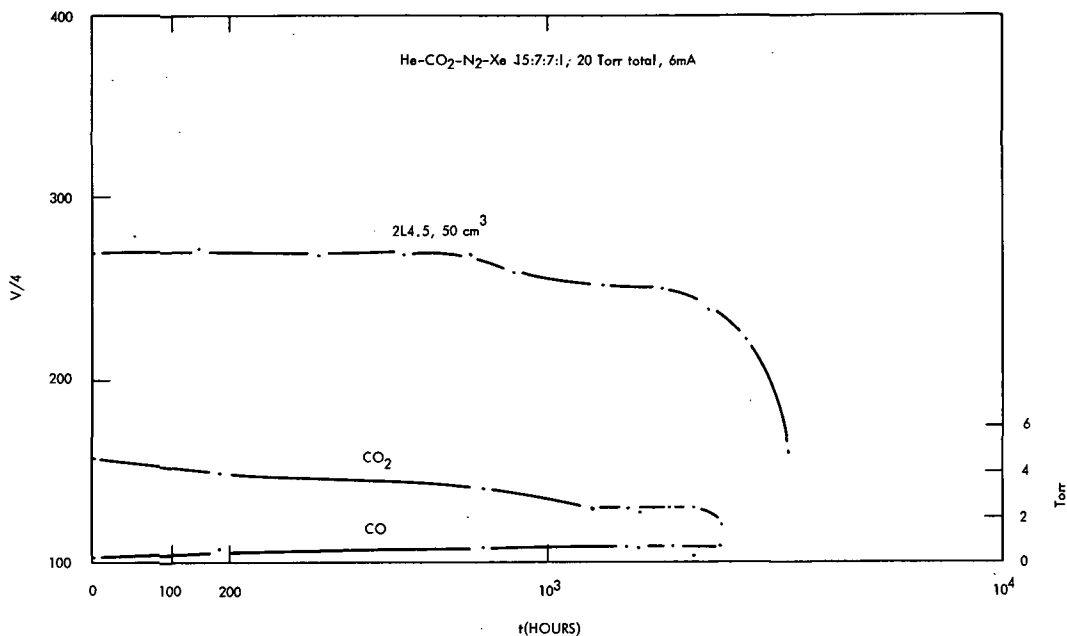


Figure 45. Silver-cadmium oxide cathode (Ag 10 Cd/O): voltage versus operating time (upper curve); CO₂ and CO partial pressures versus operating time (lower curves).

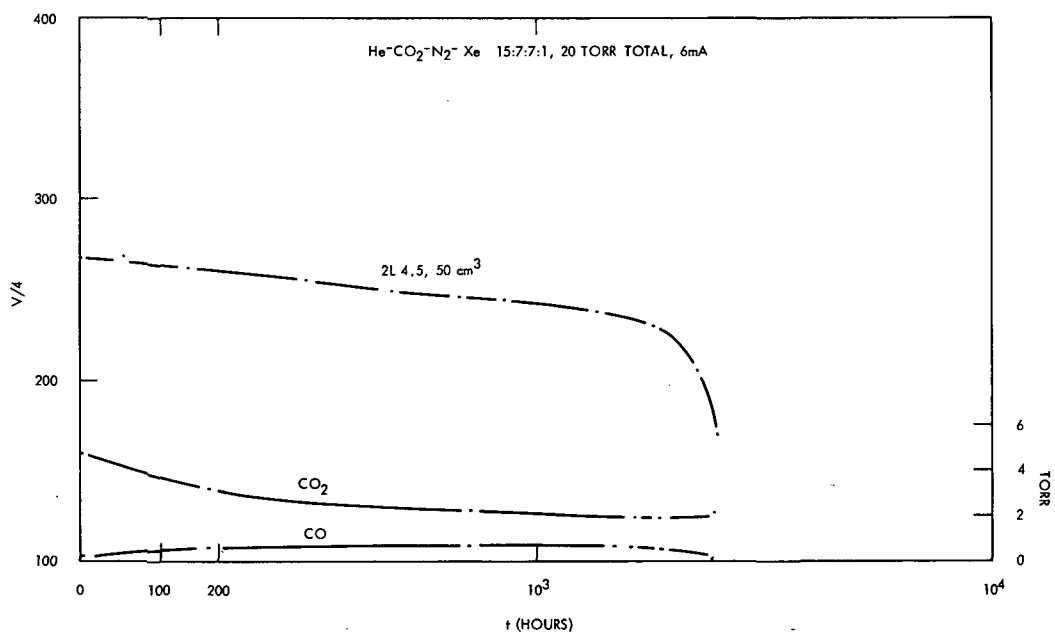


Figure 46. Silver-cadmium oxide cathode (Ag 20 Cd/O): voltage versus operating time (upper curve); CO₂ and CO partial pressures versus operating time (lower curves).

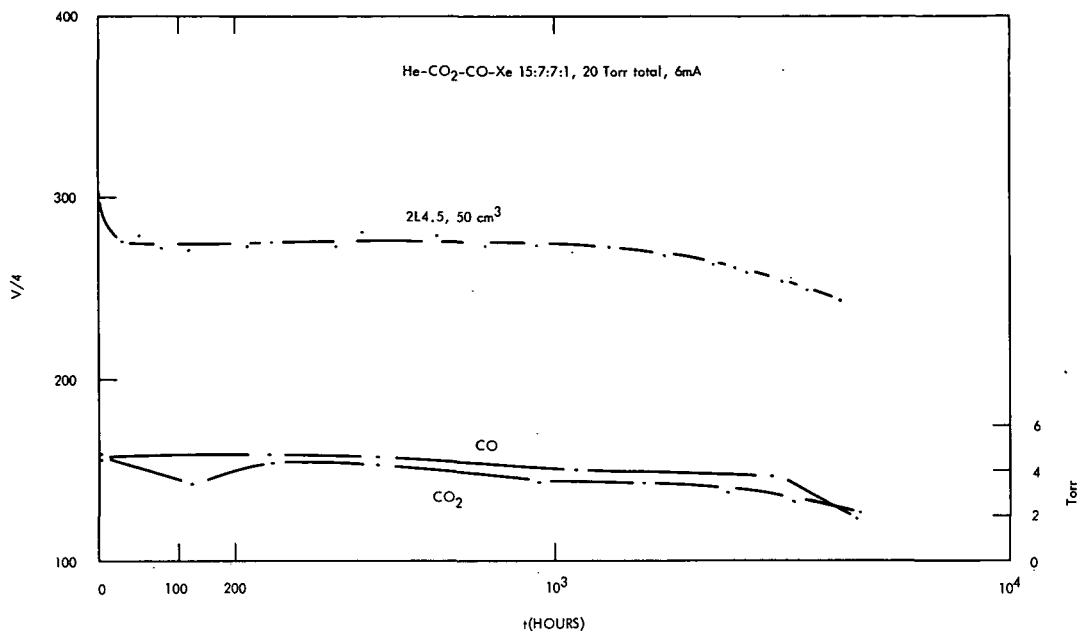


Figure 47. Silver-copper oxide insulated cathode (Ag 5 Cu/O): voltage versus operating time (upper curve); CO₂ and CO partial pressures versus operating time (lower curves).

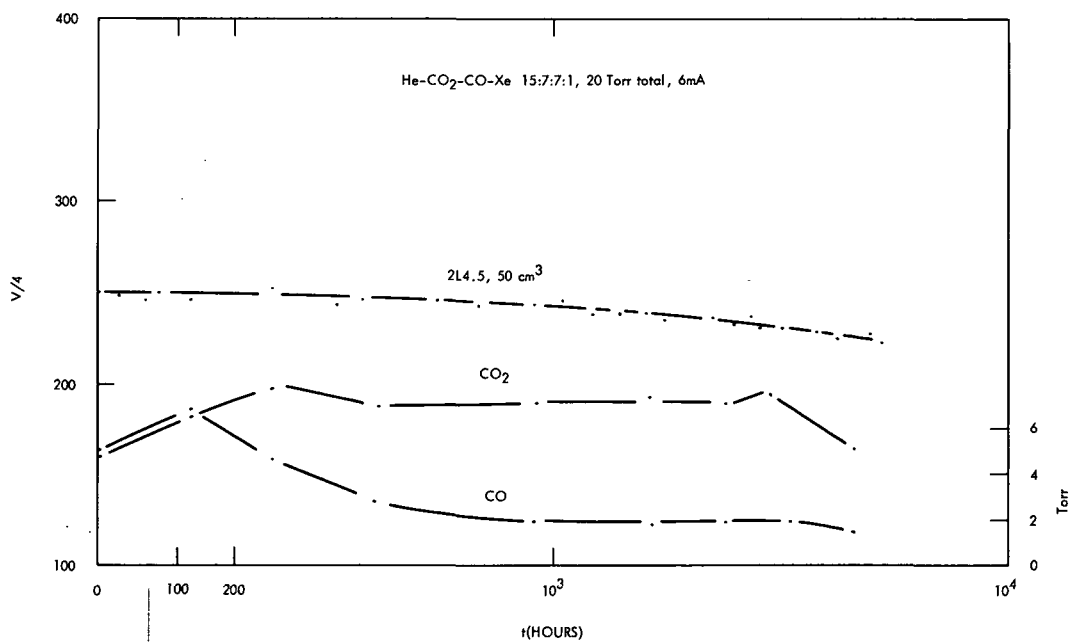


Figure 48. Silver-copper oxide insulated cathode (Ag 10 Cu/O): voltage versus operating time (upper curve); CO₂ and CO partial pressures versus operating time (lower curves).

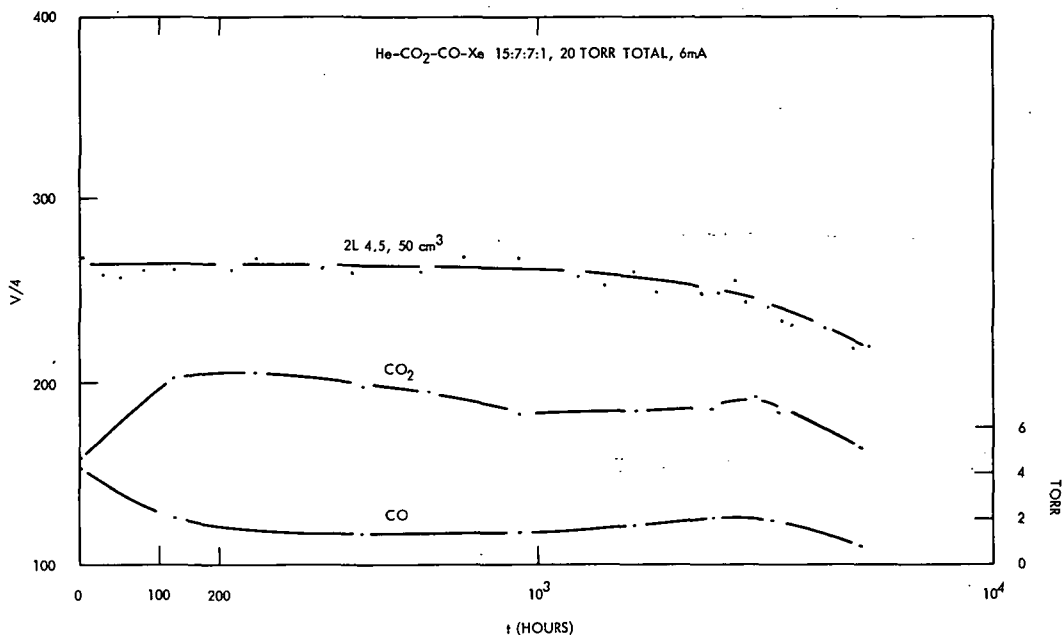


Figure 49. Silver-copper oxide insulated cathode (Ag 20 Cu/O): voltage versus operating time (upper curve); CO₂ and CO partial pressures versus operating time (lower curves).

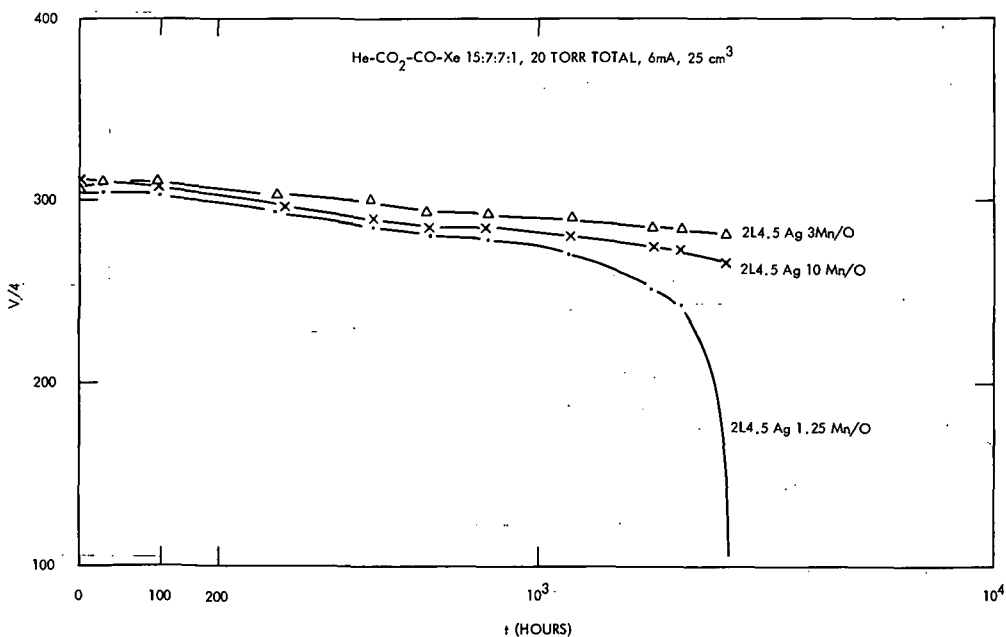


Figure 50. Silver-manganese dioxide cathodes (Ag-Mn/O): voltage versus operating time.

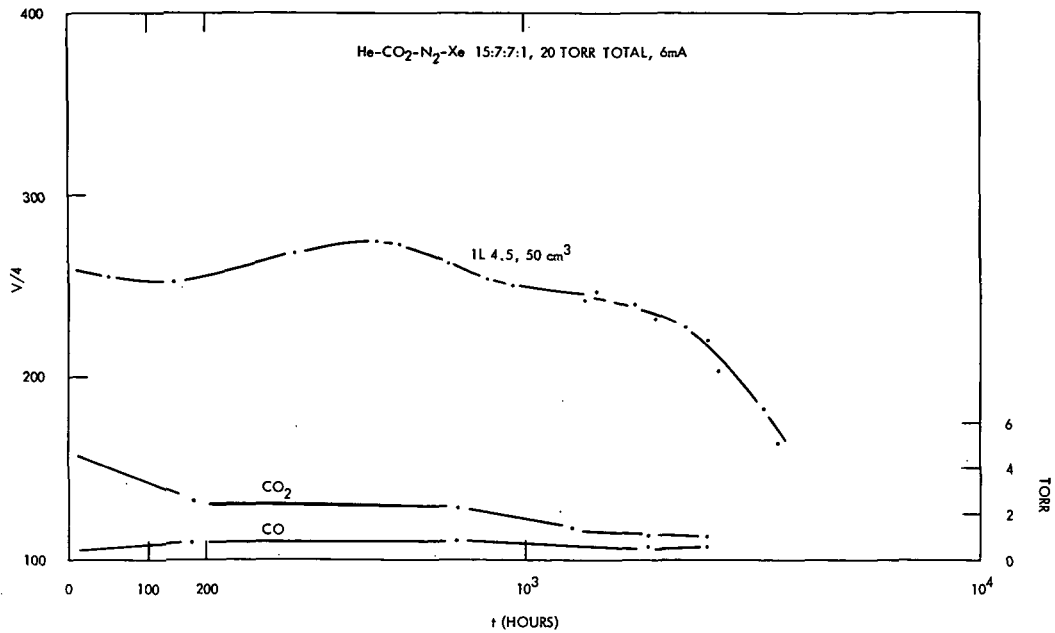


Figure 51. Silver-nickel oxide cathode (AG 15 Ni/O): voltage versus operating time (upper curve); CO₂ and CO partial pressures versus operating time (lower curves).

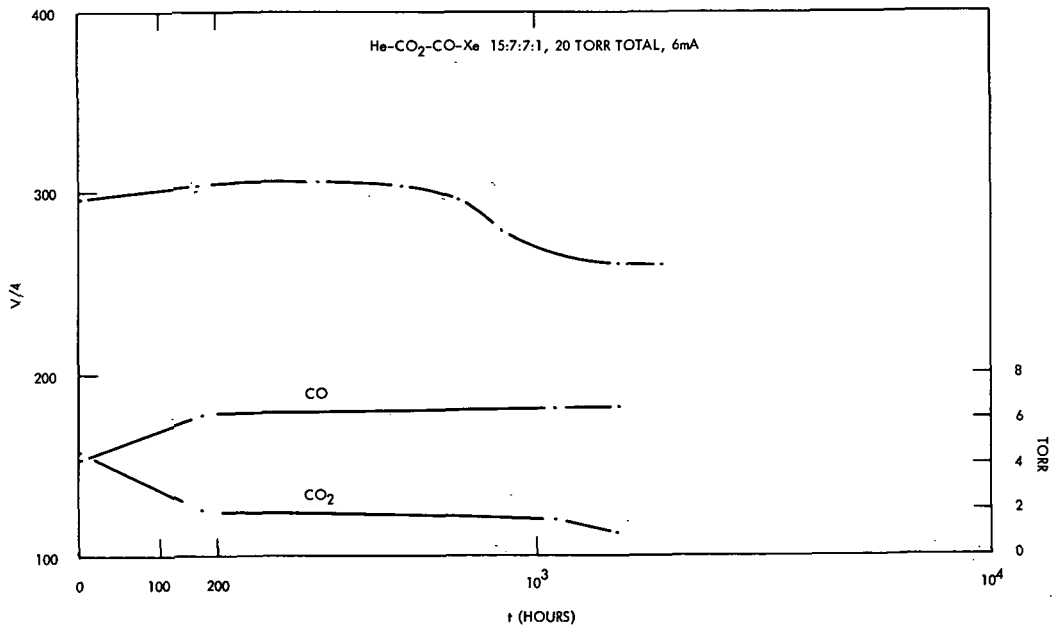


Figure 52. Silver-zinc oxide cathode (Ag 10 Zn/O): voltage versus operating time (upper curve); CO₂ and CO partial pressures versus operating time (lower curves).

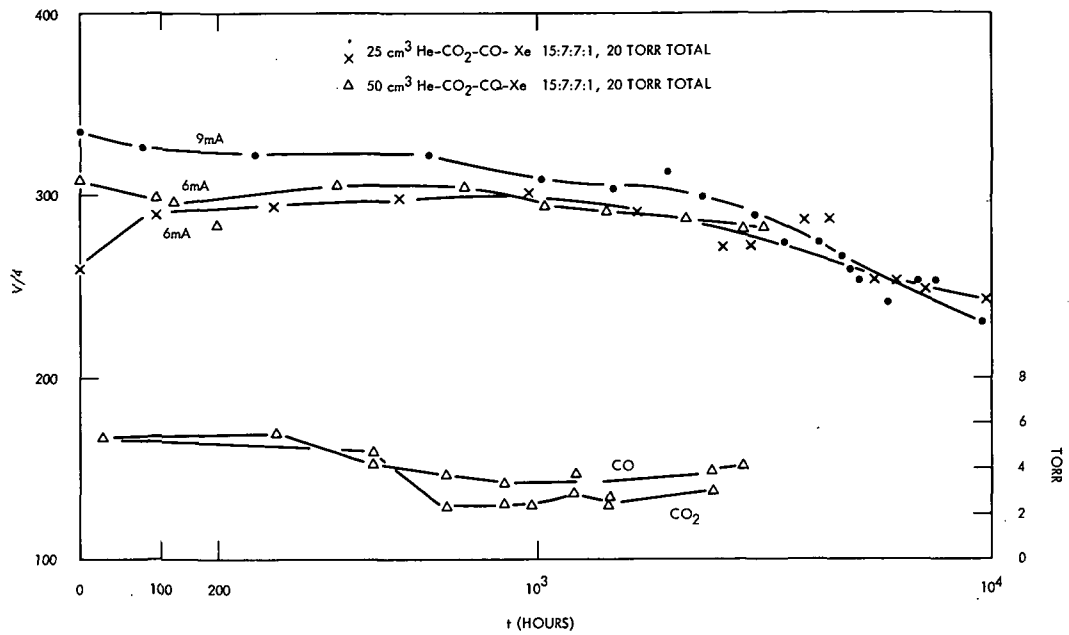


Figure 53. Copper cathodes (1L 4.5 Cu): voltage versus operating time (upper curves); CO₂ and CO partial pressures versus operating time (lower curves).

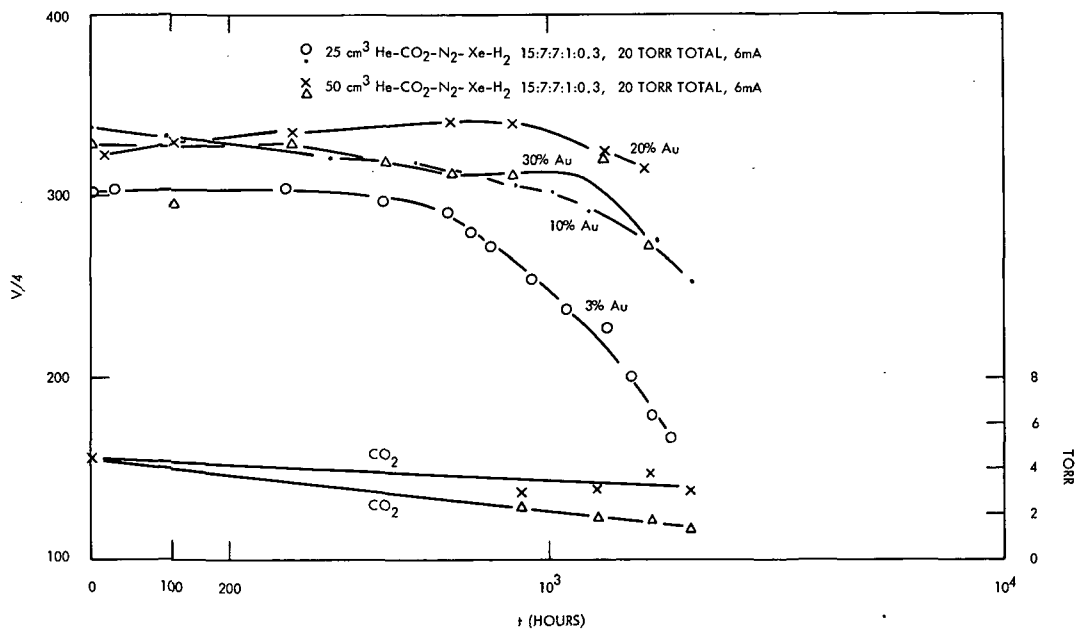


Figure 54. Platinum-gold cathodes (3L 10 Pt-Au): voltage versus operating time.

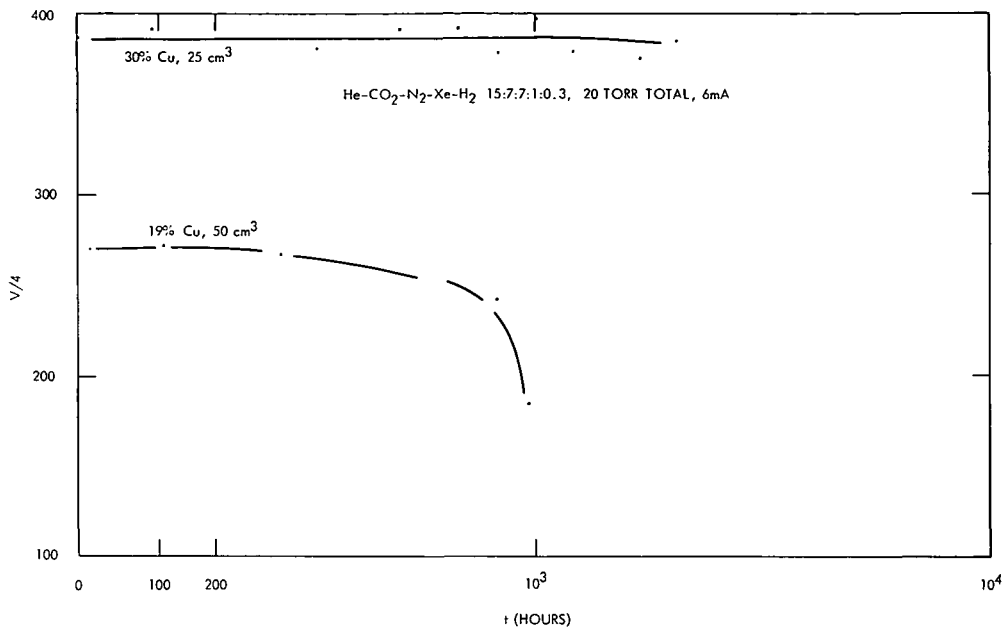


Figure 55. Platinum-copper cathodes (3L 10 Pt-Cu): voltage versus operating time.

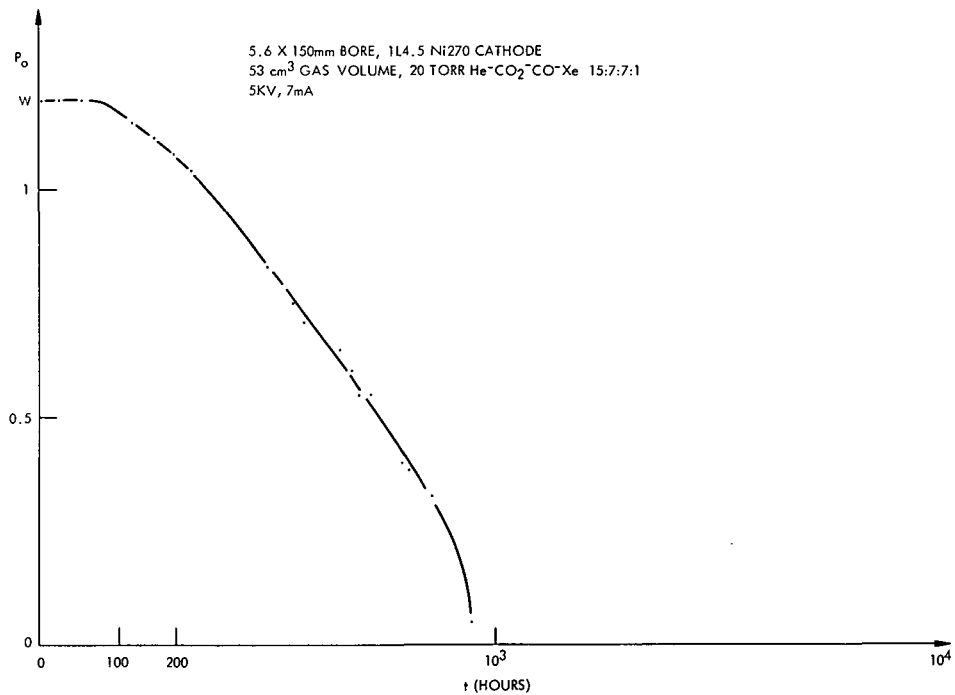


Figure 56. CO₂ laser power output versus time.

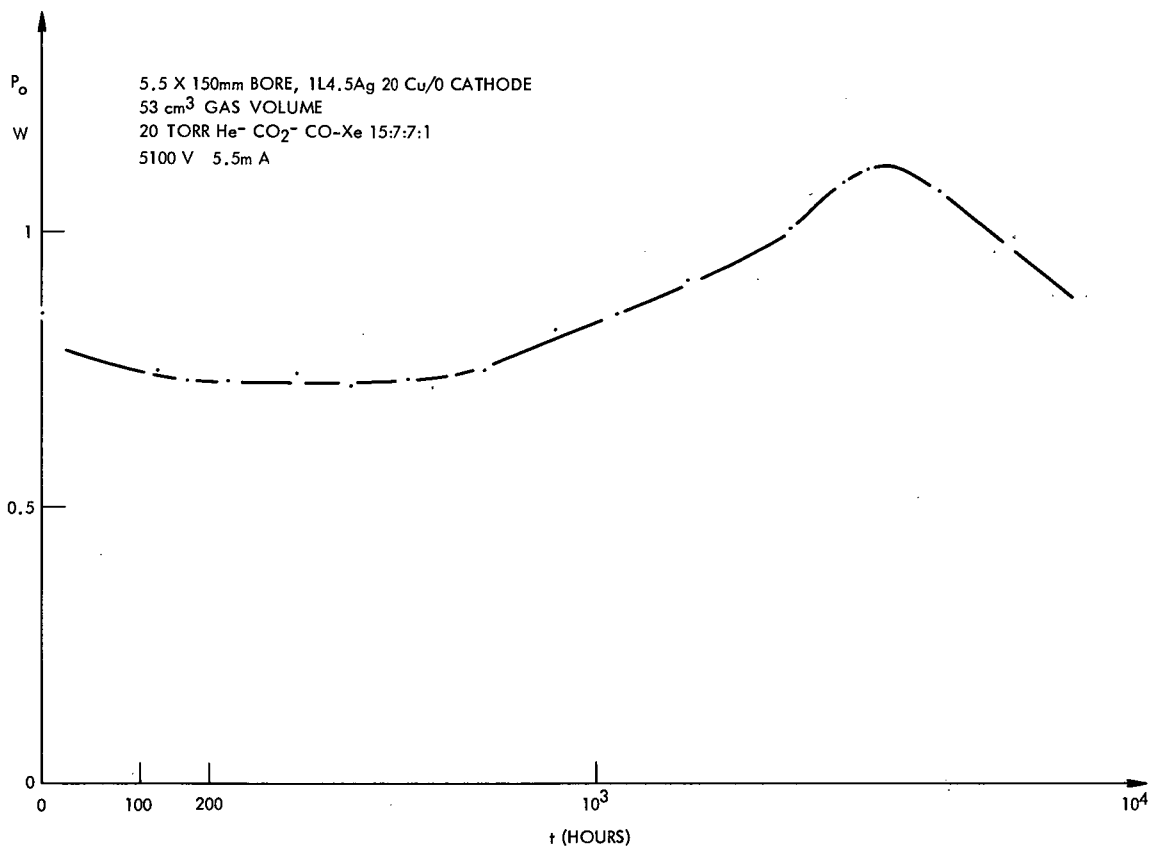


Figure 57. CO₂ laser power output versus time.

APPENDIX

LASER V-I CHARACTERISTICS AND LASER POWER OUTPUT

LASER V-I CHARACTERISTICS FOR DIFFERENT GAS MIXTURES

These characteristics are shown in Figures 1a to 26a. The voltages shown represent the values directly across the laser tube and do not include series resistance drop. Figure 27a shows the design of the laser tube. In numbering the figures in this appendix, some numbers have been omitted, in order to maintain a direct correspondence with previous figures.

LASER POWER OUTPUT FOR MIXTURES WITH LOW CO and CO₂ CONTENT

This information is shown in Figures 28a and 29a and is useful in determining the laser output near the end of the life, when the CO₂ and CO concentrations have fallen off from their initial values.

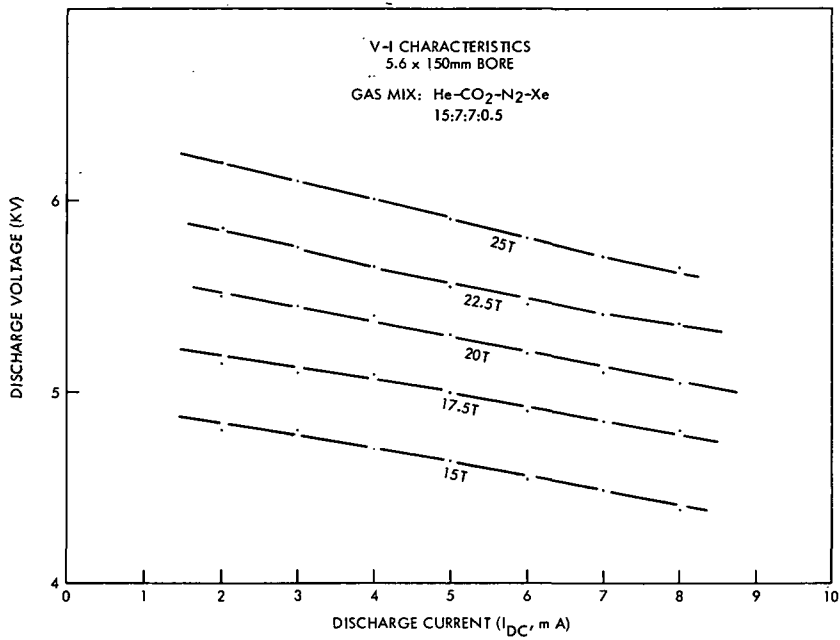


Figure 1a. Discharge current (I_{DC} , mA).

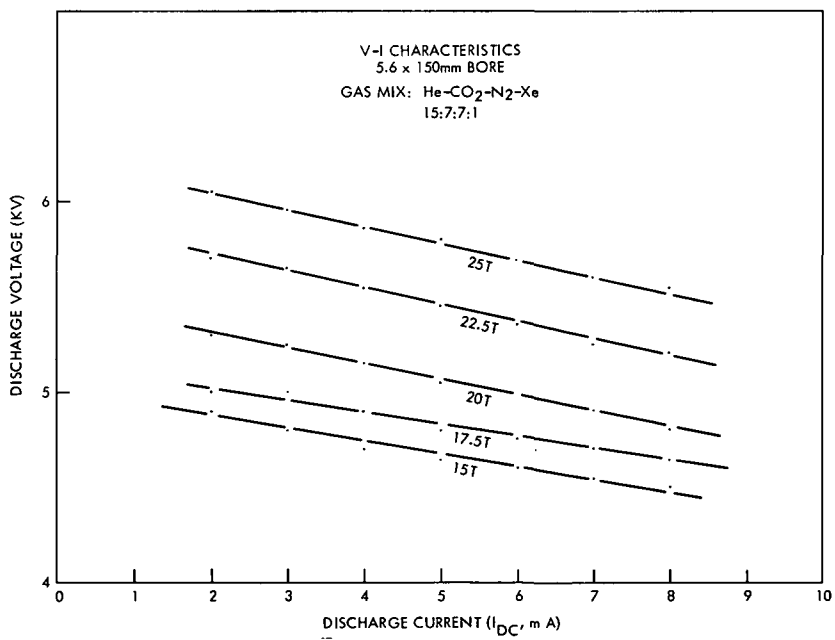


Figure 2a. Discharge current (I_{DC} , mA).

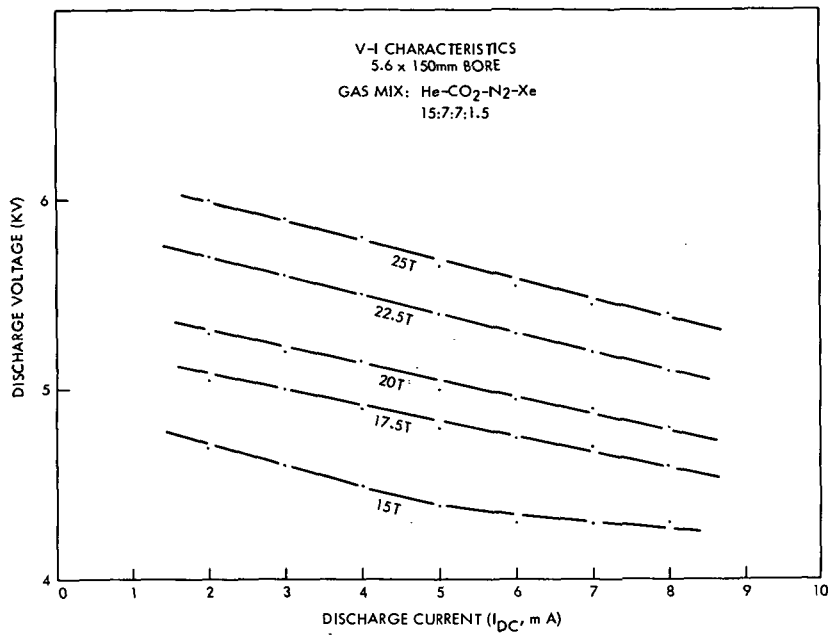


Figure 3a. Discharge current (I_{DC} , mA).

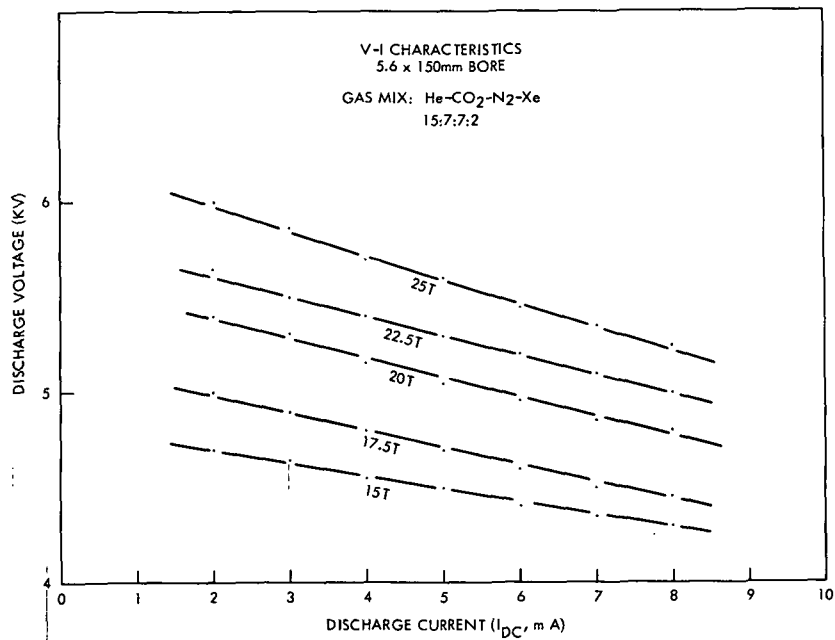


Figure 4a. Discharge current (I_{DC} , mA).

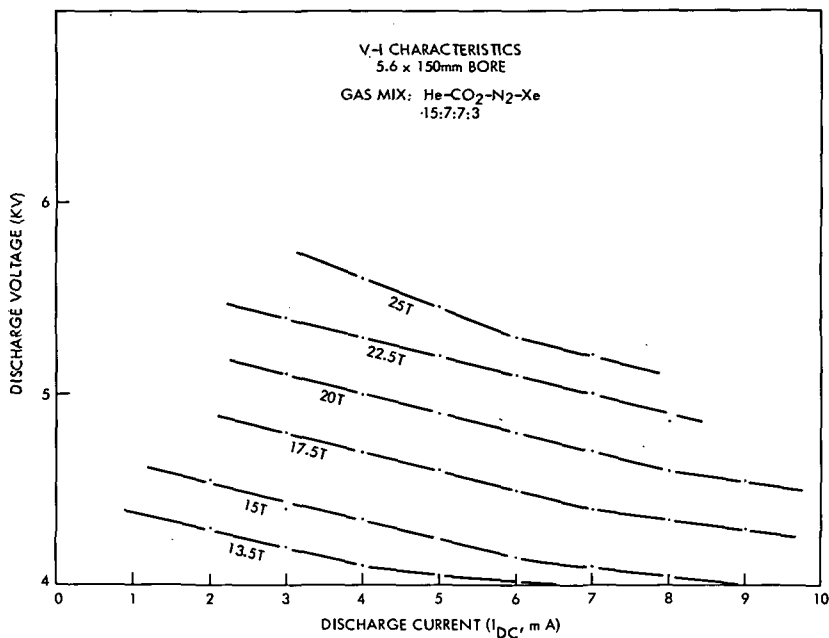


Figure 5a. Discharge current (I_{DC} , mA).

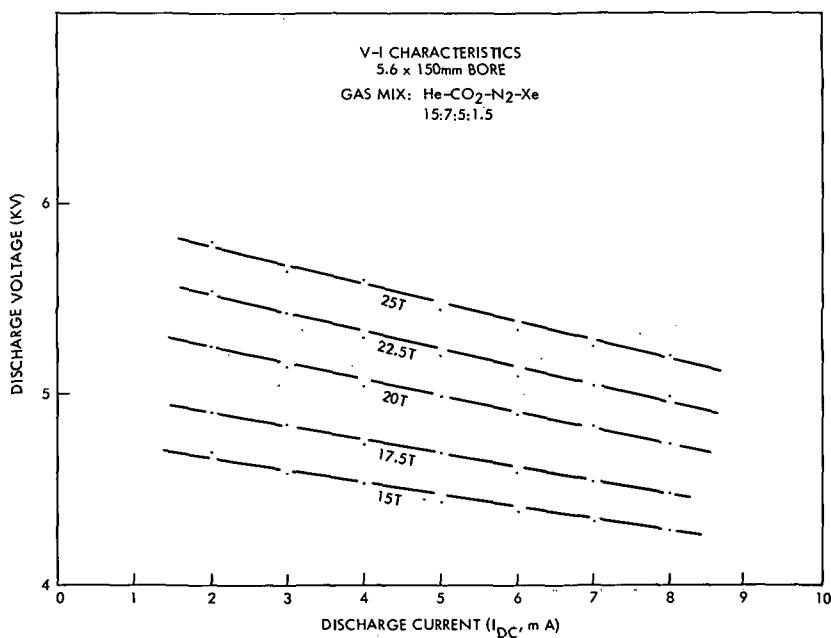


Figure 6a. Discharge current (I_{DC} , mA).

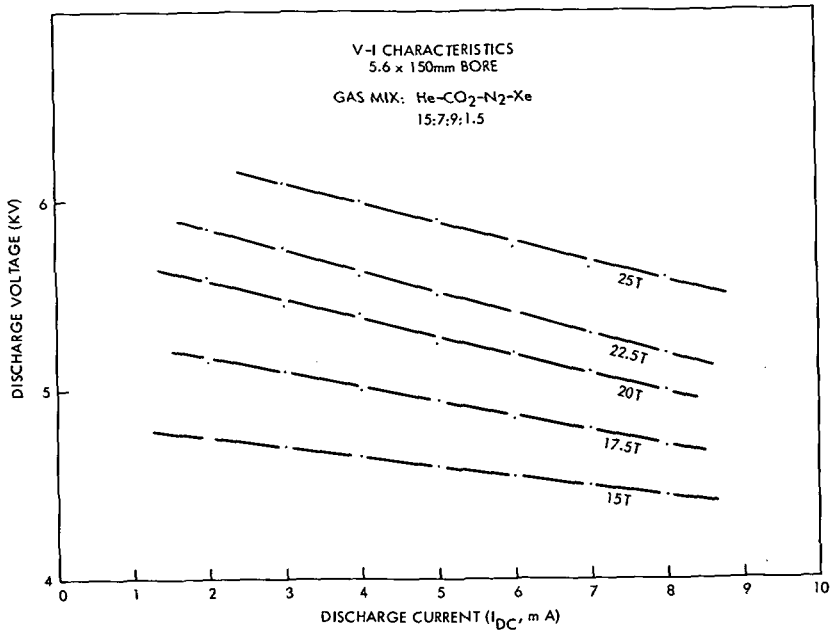


Figure 8a. Discharge current (I_{DC}, mA).

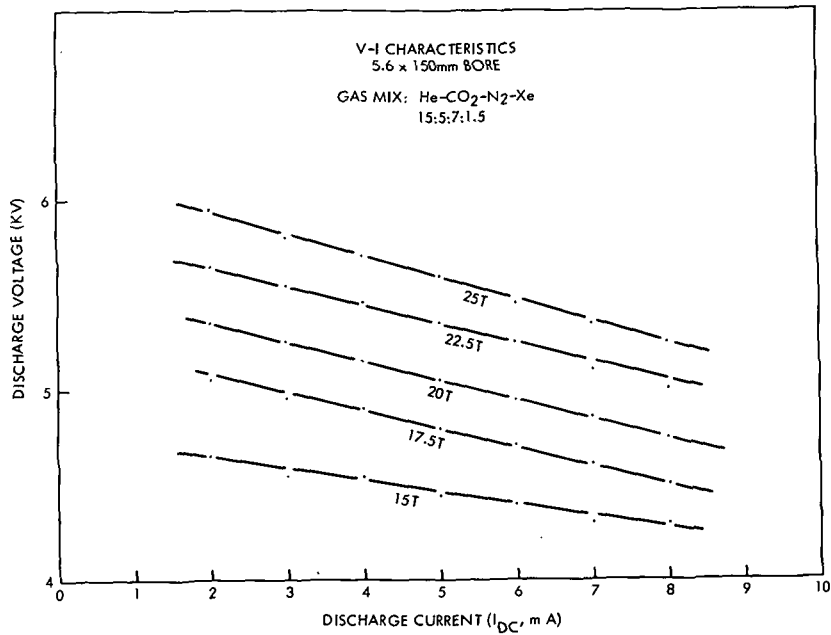


Figure 9a. Discharge current (I_{DC}, mA).

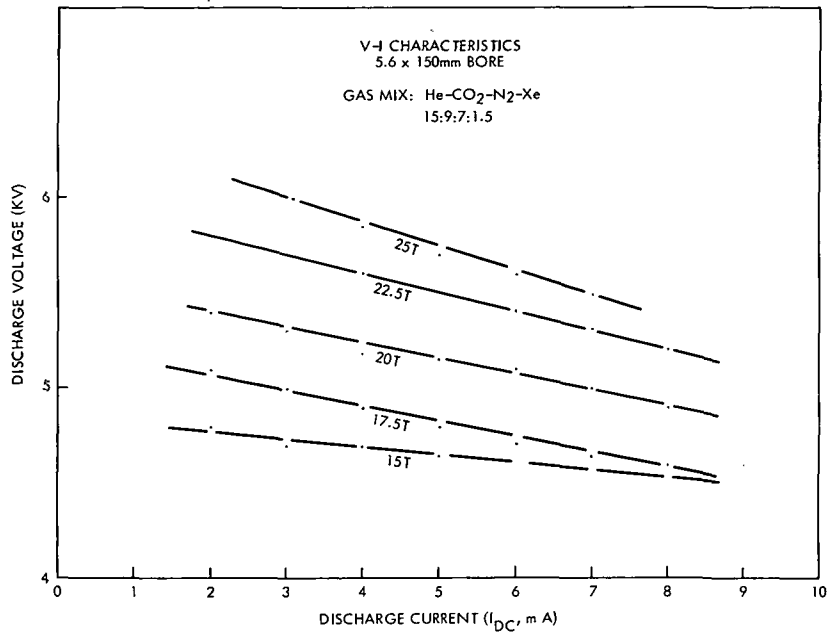


Figure 11a. Discharge current (I_{DC} , mA).

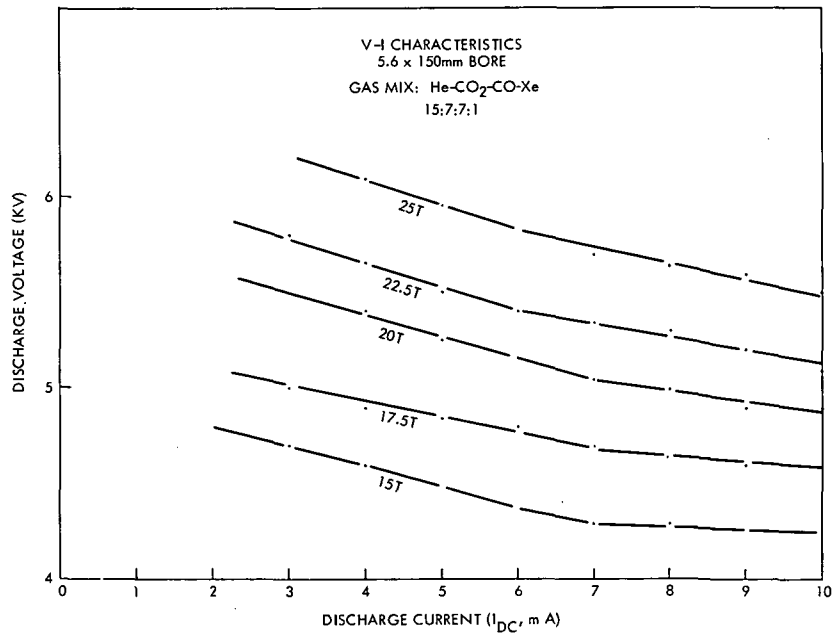


Figure 12a. Discharge current (I_{DC} , mA).

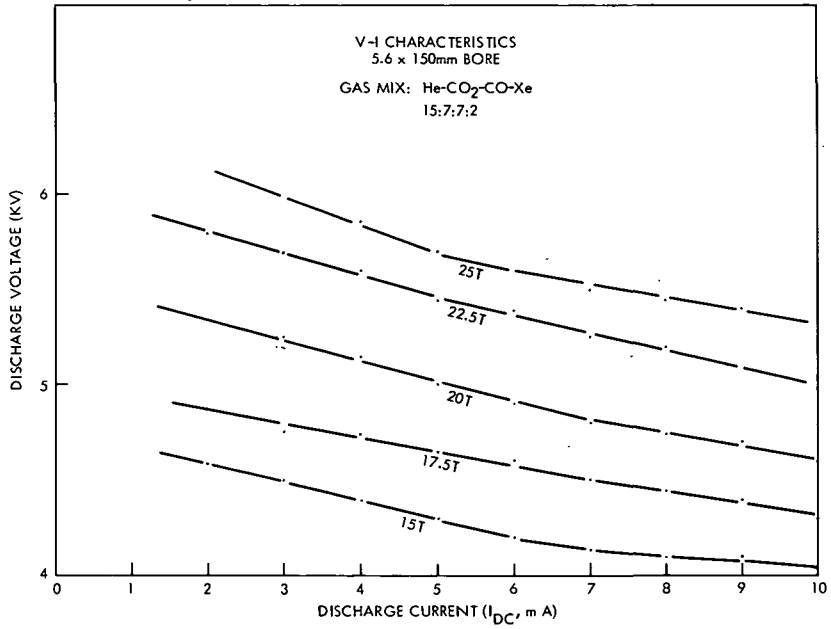


Figure 13a. Discharge current (I_{DC} , mA).

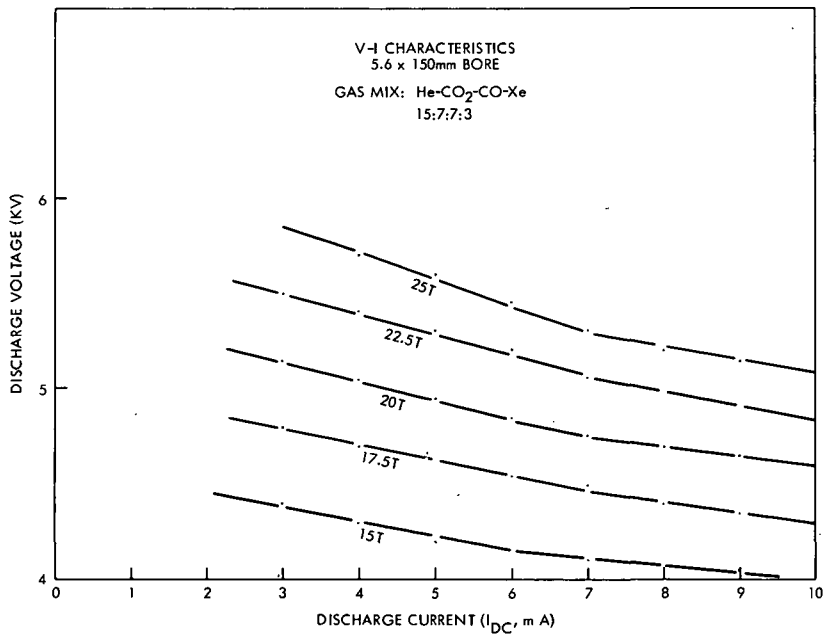


Figure 14a. Discharge current (I_{DC} , mA).

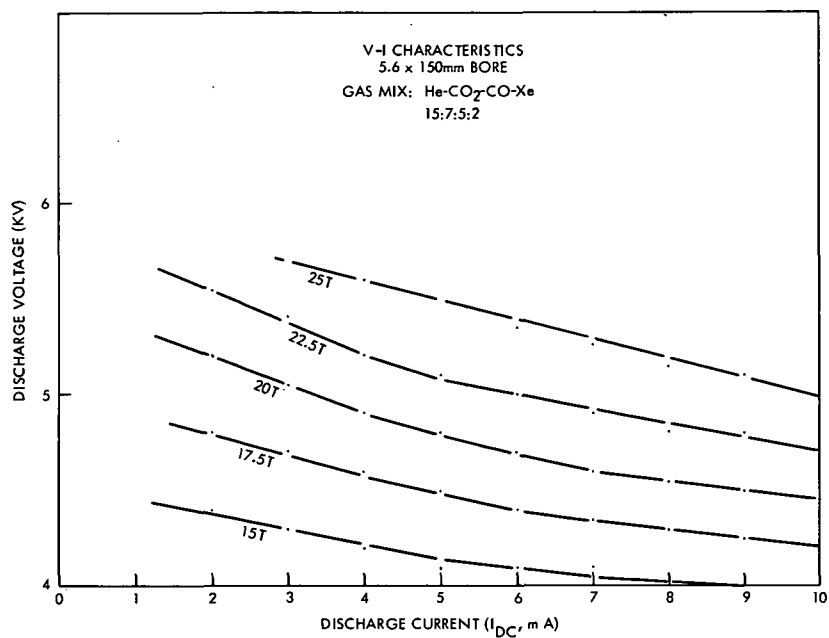


Figure 15a. Discharge current (I_{DC} , mA).

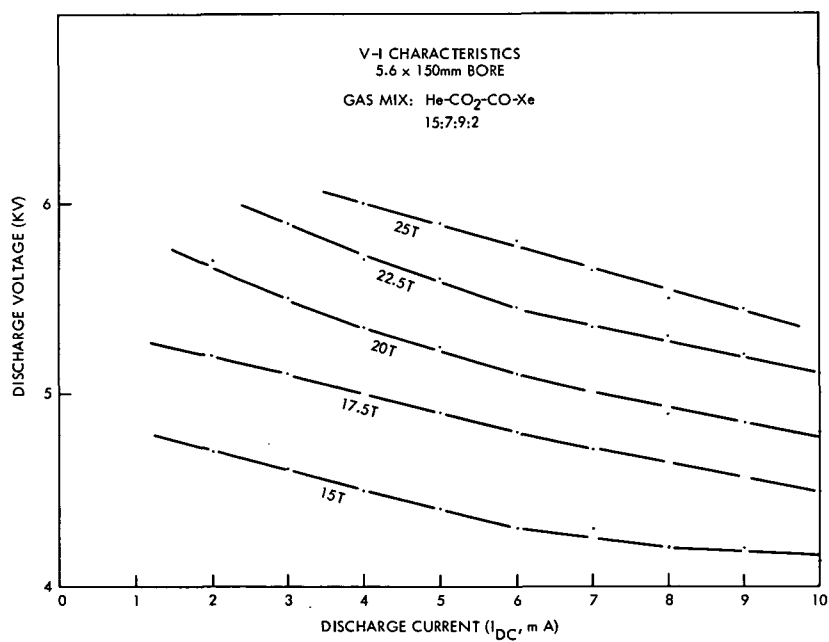


Figure 17a. Discharge current (I_{DC} , mA).

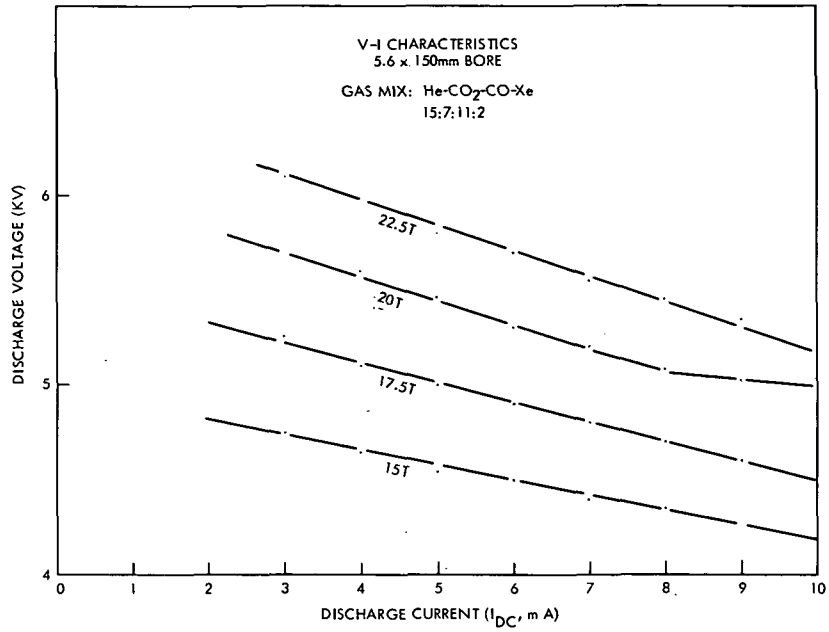


Figure 18a. Discharge current (I_{DC}, mA).

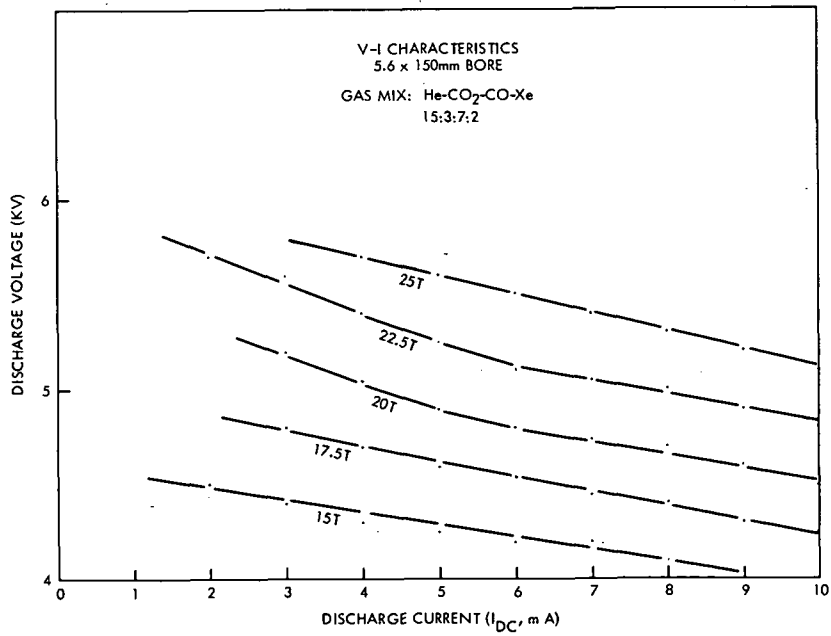


Figure 19a. Discharge current (I_{DC}, mA).

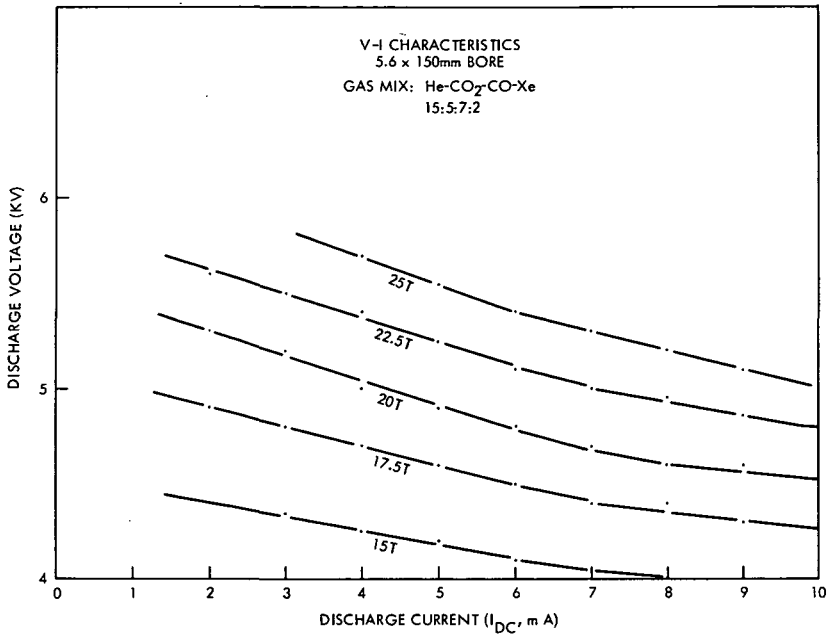


Figure 20a. Discharge current (I_{DC} , mA).

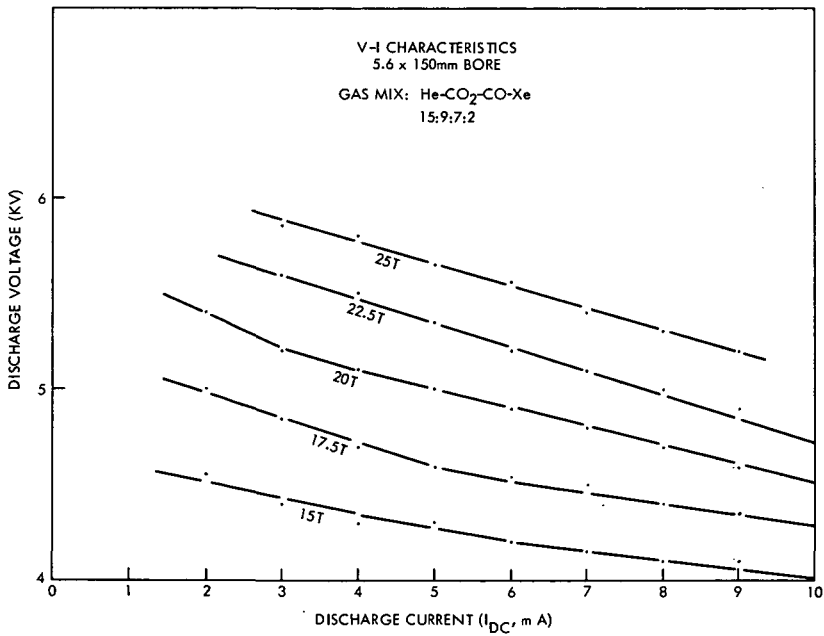


Figure 22a. Discharge current (I_{DC} , mA).

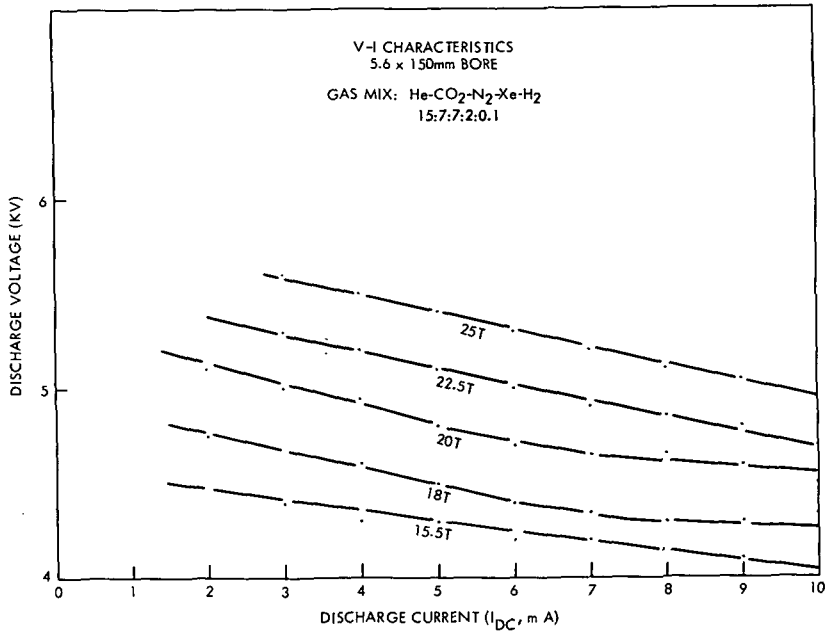


Figure 24a. Discharge current (I_{DC} , mA).

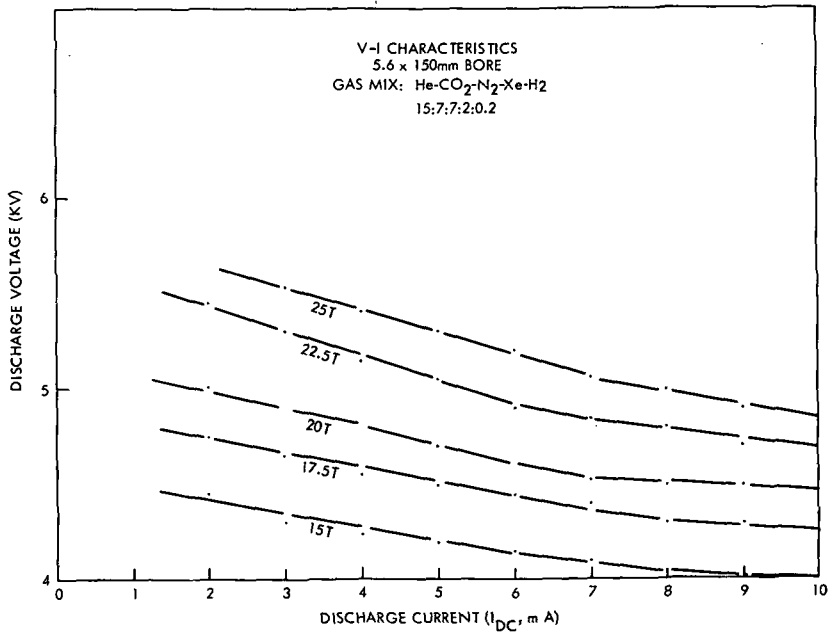


Figure 25a. Discharge current (I_{DC} , mA).

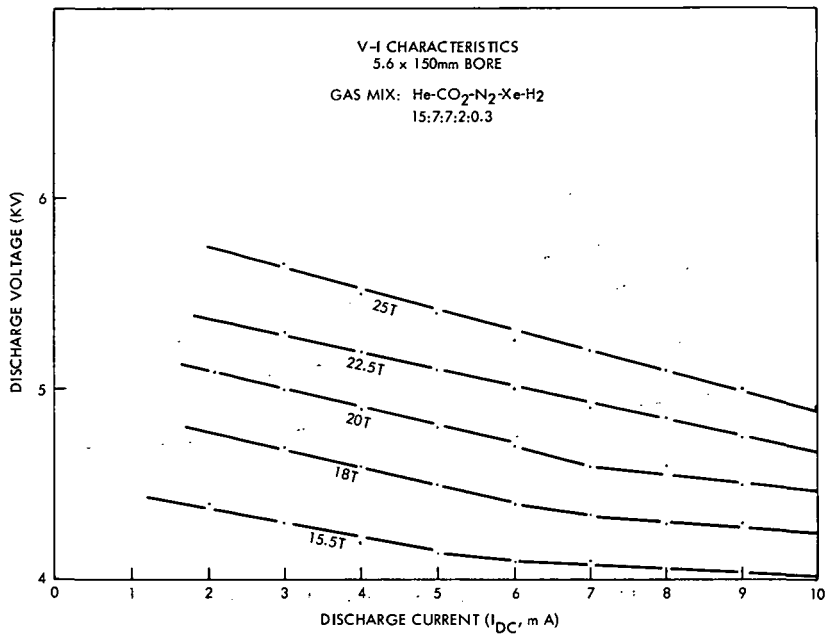


Figure 26a. Discharge current (I_{DC} , mA).

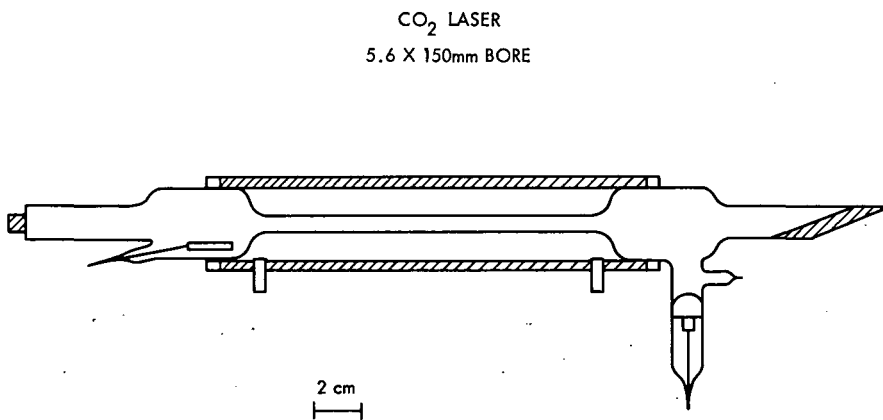


Figure 27a. CO₂ laser; 5.6 X 150 mm bore.

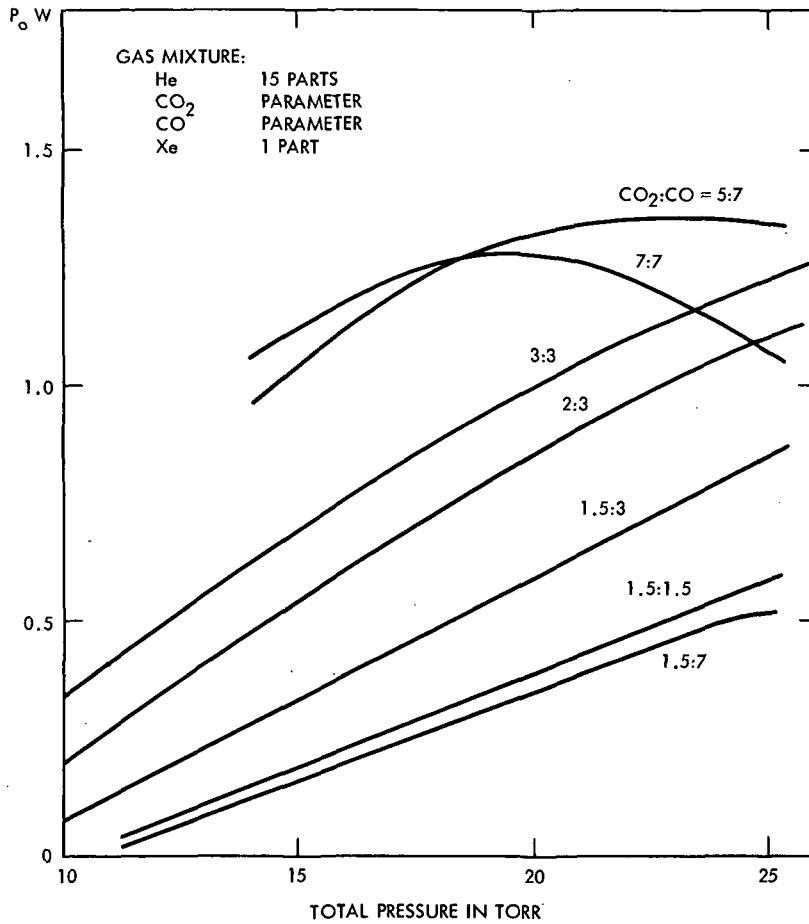


Figure 28a. Power output versus total pressure 5.6 X 150 mm bore, 6 mA DC.

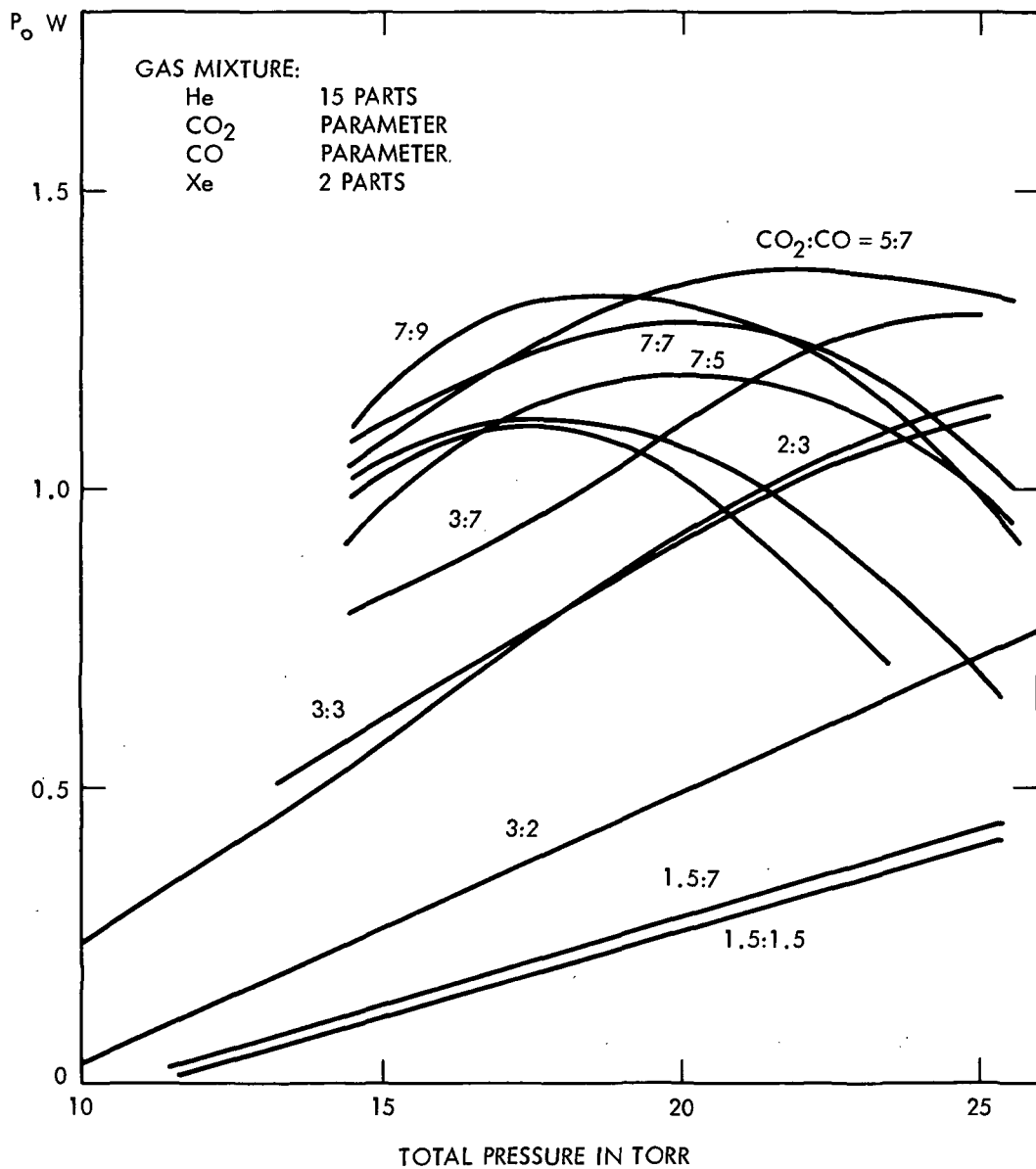


Figure 29a. Power output versus total pressure 5.6 X 150 mm bore, 6 mA DC.



POSTMASTER: If Undeliverable (Section 158
Postal Manual) Do Not Return

"The aeronautical and space activities of the United States shall be conducted so as to contribute . . . to the expansion of human knowledge of phenomena in the atmosphere and space. The Administration shall provide for the widest practicable and appropriate dissemination of information concerning its activities and the results thereof."

—NATIONAL AERONAUTICS AND SPACE ACT OF 1958

NASA SCIENTIFIC AND TECHNICAL PUBLICATIONS

TECHNICAL REPORTS: Scientific and technical information considered important, complete, and a lasting contribution to existing knowledge.

TECHNICAL NOTES: Information less broad in scope but nevertheless of importance as a contribution to existing knowledge.

TECHNICAL MEMORANDUMS: Information receiving limited distribution because of preliminary data, security classification, or other reasons. Also includes conference proceedings with either limited or unlimited distribution.

CONTRACTOR REPORTS: Scientific and technical information generated under a NASA contract or grant and considered an important contribution to existing knowledge.

TECHNICAL TRANSLATIONS: Information published in a foreign language considered to merit NASA distribution in English.

SPECIAL PUBLICATIONS: Information derived from or of value to NASA activities. Publications include final reports of major projects, monographs, data compilations, handbooks, sourcebooks, and special bibliographies.

TECHNOLOGY UTILIZATION PUBLICATIONS: Information on technology used by NASA that may be of particular interest in commercial and other non-aerospace applications. Publications include Tech Briefs, Technology Utilization Reports and Technology Surveys.

Details on the availability of these publications may be obtained from:

SCIENTIFIC AND TECHNICAL INFORMATION OFFICE

NATIONAL AERONAUTICS AND SPACE ADMINISTRATION

Washington, D.C. 20546